RNA-Seq Alignment to Individualized Genomes Improves Transcript Abundance Estimates in Multiparent Populations

Steven C. Munger,* Narayanan Raghupathy,* Kwangbom Choi,* Allen K. Simons,* Daniel M. Gatti,* Douglas A. Hinerfeld,* Karen L. Svenson,* Mark P. Keller,† Alan D. Attie,† Matthew A. Hibbs,*,‡ Joel H. Graber,* Elissa J. Chesler,* and Gary A. Churchill*,[1]

*The Jackson Laboratory, Bar Harbor, Maine 04609, †University of Wisconsin, Madison, Wisconsin 53705, and ‡Trinity University, San Antonio, Texas 78212

ORCID ID: 0000-0002-8458-1871 (S.C.M.)

ABSTRACT Massively parallel RNA sequencing (RNA-seq) has yielded a wealth of new insights into transcriptional regulation. A first step in the analysis of RNA-seq data is the alignment of short sequence reads to a common reference genome or transcriptome. Genetic variants that distinguish individual genomes from the reference sequence can cause reads to be misaligned, resulting in biased estimates of transcript abundance. Fine-tuning of read alignment algorithms does not correct this problem. We have developed Seqnature software to construct individualized diploid genomes and transcriptomes for multiparent populations and have implemented a complete analysis pipeline that incorporates other existing software tools. We demonstrate in simulated and real data sets that alignment to individualized transcriptomes increases read mapping accuracy, improves estimation of transcript abundance, and enables the direct estimation of allele-specific expression. Moreover, when applied to expression QTL mapping we find that our individualized alignment strategy corrects false-positive linkage signals and unmasks hidden associations. We recommend the use of individualized diploid genomes over reference sequence alignment for all applications of high-throughput sequencing technology in genetically diverse populations.

RNA sequencing (RNA-seq) has transformed our understanding of gene expression and transcriptional regulation (Lister *et al.* 2008; Mortazavi *et al.* 2008; Nagalakshmi *et al.* 2008; Wang *et al.* 2009). Alignment of short read sequences (reads) is a critical first step in the analysis of an RNA-seq experiment. The most widely used alignment strategies rely on a reference genome, a single haploid sequence that serves as the representative for a genetically diverse species. For example, the mouse reference genome is derived from the C57BL/6J inbred strain (Mouse Genome Sequencing Consortium 2002). Polymorphisms in individual RNA samples will generate reads that differ from the reference genome. These differences are indistinguishable from sequencing errors in the read-alignment step where alignment algorithms allow for mismatches and small insertions or deletions (indels). Polymorphisms can be distinguished from sequencing errors in *post hoc* analysis of the multiple-read alignments (McKenna *et al.* 2010) when the read alignments are assumed to be correct. However, polymorphisms have a demonstrated potential to create systematic errors in alignment that can affect many reads and lead to biases in the quantification of transcript abundance (Degner *et al.* 2009). Known variants can be masked or substituted in the reference genome (Satya *et al.* 2012) but this strategy discards important information that can aid correct read alignment.

The target of read alignment can be a whole genome or only the transcribed portion of the genome (transcriptome). Whole-genome alignment must allow for reads that span splice junctions; specialized alignment algorithms have been developed to address this problem (Li and Durbin 2009; Trapnell *et al.* 2009, 2010; Wu and Nacu 2010). Transcriptome alignment substantially reduces target complexity by limiting it to known transcripts, including all possible splice isoforms (Li and Dewey 2011).

doi: 10.1534/genetics.114.165886
Manuscript received May 5, 2014; accepted for publication June 4, 2014
Available freely online through the author-supported open access option.
Supporting information is available online at http://www.genetics.org/lookup/suppl/doi:10.1534/genetics.114.165886/-/DC1.

[1] Corresponding author: The Jackson Laboratory, 600 Main St., Bar Harbor, ME 04609. E-mail: gary.churchill@jax.org

The genomes of most organisms include gene families and transcribed pseudogenes with varying degrees of sequence similarity. As a result, it is not always possible to obtain a single unique alignment for a given read. Genomic regions consisting of common or repeat sequences that prevent unique read alignment are said to have low *mappability* (Derrien *et al.* 2012; Graze *et al.* 2012; Stevenson *et al.* 2013). We refer to reads that align to multiple such locations in the genome as *genomic multireads*. Transcriptomes include multiple isoforms with shared exons. Thus reads that align uniquely in the genomic sequence can be shared by two or more isoforms. We refer to these as *isoform multireads*. When the alignment target is diploid, consisting of two copies of a genome or transcriptome, reads may align equally well to both copies. We refer to these as *allelic multireads*. A given read may belong to one or more of these classes of multireads simultaneously. However, it is assumed that each read is derived uniquely from one gene, isoform, and allele. Appropriate methods for resolving the probable origin of multireads are key to obtaining accurate transcript abundance estimates (Mortazavi *et al.* 2008). Restricting attention to only uniquely mapping reads is problematic, as we illustrate below.

Quantification of transcript abundance is based on partitioning of the target genome or transcriptome into discrete units, which may be genes, isoforms, exons, or allelic copies of any of these. The posterior probability that a read originated from one of the loci to which it aligns can be computed using an expectation-maximization (EM) algorithm (Li *et al.* 2010; Nicolae *et al.* 2011; Roberts and Pachter 2013; Patro *et al.* 2014). The probabilities serve as weights that sum to one for each read and relative abundance is estimated as the sum of weights for all reads that align to that locus. In this way, a read may be aligned to more than one locus but the total weight contributed by the read is one. In this work we align reads to the transcriptome at the isoform level and we summarize transcript abundance at the gene level. Alignment to the transcriptome allows us to capture junction-spanning reads and to apply appropriate length adjustments. However, we find that the precision with which we can estimate isoform proportions is low with current sequencing technologies and therefor focus on estimates of gene-level abundance. Gene-level abundance is computed as the sum of the estimated transcript counts across all isoforms of the gene.

In outbred populations, heterozygous sites are informative for allele-specific expression. Current approaches to analysis of allele-specific expression from RNA-seq construct two haploid genome sequences corresponding to the two parents (McManus *et al.* 2010; Rivas-Astroza *et al.* 2011; Rozowsky *et al.* 2011; Graze *et al.* 2012; Shen *et al.* 2013). Reads are aligned sequentially to the haploid maternal and paternal genomes and reads that map uniquely to one parent are used to estimate allelic imbalance. Bayesian hierarchical models can be used to test allelic imbalance across multiple SNPs within a gene (Skelly *et al.* 2011). These methods discard allelic multireads that map to both parents and fail to account for reads that are simultaneously genomic and allelic multireads. Including all reads by allocating the allelic multireads using an EM algorithm improves the accuracy of allele-specific expression (Turro *et al.* 2011). We adopt a similar approach here.

The focus of this work is to evaluate the impact of individualized genomes on transcript quantification. Toward this end we have made what we regard to be a reasonable choice in the methods used to quantify aligned reads. We evaluate the impact of alignment to individualized diploid genomes on RNA-seq analysis with an emphasis on experimental multiparent populations. We have developed the Seqnature software to construct individualized genomes and transcriptomes for inbred strains and multiparent populations, including the Diversity Outbred (DO)—a multiparent population derived from eight inbred mouse strains (Churchill *et al.* 2012; Svenson *et al.* 2012). Seqnature performs two main functions. For inbred strains, Seqnature incorporates SNPs and small indels (<100 bp) into a reference genome to create a strain-specific genome sequence. For multiparent populations, Seqnature uses inferred founder haplotypes to construct a pair of individualized haploid genome sequences incorporating known SNPs and indels from the founder strains. The software merges these two sequences to produce an individualized diploid genome. Seqnature also modifies gene annotation files to account for coordinate offsets from indels and constructs a diploid transcriptome file in a format suitable for RNA-seq read alignment.

We incorporate Seqnature into an RNA-seq analysis pipeline that uses existing software for read alignment [Bowtie (Langmead *et al.* 2009)] and quantification [RSEM (Li and Dewey 2011)]. Other software tools can be substituted into this pipeline. We demonstrate, using real and simulated data, that individualized transcriptomes improve the accuracy of read alignment and quantification. The Seqnature pipeline provides direct estimates of allele-specific expression for genes with heterozygosity. We demonstrate that in expression quantitative trait locus (eQTL) mapping, read alignment to individualized transcriptomes reduces the number of spurious linkages and unmasks extensive local genetic variation affecting gene expression.

Materials and Methods

Animals

Male and female Diversity Outbred mice (J:DO stock no. 009376) were obtained from The Jackson Laboratory (JAX, Bar Harbor, ME). Animals were received at 3 weeks of age, housed at JAX, and given free access to either standard rodent chow containing 6% fat by weight (LabDiet 5K52; LabDiet, Scott Distributing) or a high-fat, high-sucrose diet containing 44.6% kcal from fat and 34% (by weight) sucrose (TD.08811) from wean age throughout the study. DO mice were phenotyped for multiple metabolic and hematological parameters as described in Svenson *et al.* (2012). At 26 weeks of age, liver samples were collected from each animal and stored in RNAlater solution (Life Technologies) at −80°.

All procedures on DO mice were approved by the Animal Care and Use Committee at JAX.

Breeder pairs of each of the eight DO founder strains were obtained from JAX, housed at the University of Wisconsin (Madison, WI), and used to generate male pups that were utilized for our study. To supplement this breeding, male mice for CAST/EiJ and NZO/HlLtJ were obtained from JAX at ~3 weeks of age. Beginning at 4 weeks of age and maintained throughout the study, mice were given free access to either a semipurified control diet containing 16.8% kcal from fat (TD.08810) or a high-fat, high-sucrose diet containing 44.6% kcal from fat and 34% (by weight) sucrose (TD.08811). With the exception of NZO/HlLtJ (NZO) mice, animals were killed at 26 weeks of age, and liver samples were collected, snap frozen, and shipped on dry ice to JAX for RNA-seq analysis. Due to a high level of lethality of NZO mice that were maintained on the high-fat/high-sucrose diet, all NZO mice were killed at 20 weeks of age. All animal procedures were approved by the Animal Care and Use Committee at the University of Wisconsin.

RNA sequencing

Total RNA was isolated from livers of 26-week-old mice and quantitated by single-end RNA sequencing. Male mice from the DO founder strains ($n = 128$ total, eight biological replicates for each strain:diet group) and both male and female DO mice ($n = 277$) were profiled. Total liver RNA was isolated using the Trizol Plus RNA extraction kit (Life Technologies) with on-column DNase digestion, and then messenger RNA (mRNA) was purified from total RNA, using biotin-tagged poly(dT) oligonucleotides and streptavidin beads. The mRNA was then fragmented and double-stranded cDNA was generated by random hexamer priming. Indexed mRNA-seq libraries were generated from 1 μg total RNA following the Illumina TruSeq standard unstranded protocol and then checked for quality and quantitated with the Agilent Bioanalyzer and the Kapa Biosystems qPCR library quantitation method. Finally, 100-bp single-end reads were generated on the Illumina HiSeq 2000. To minimize technical variation, samples were randomly assigned to lanes, barcoded, and multiplexed at 12–24× per lane, and two to four technical replicates for each DO sample were sequenced. Base calls were performed using CASAVA v1.8.0, and fragmented fastq files were concatenated and then filtered to remove low-quality reads, using the Illumina CASAVA-1.8 Fastq Filter.

Construction of individualized genomes and transcriptomes

High-confidence SNPs and indels of <100 bases from the DO founder strains were obtained from the Sanger Mouse Genomes website [(Keane *et al.* 2011) Release 20111102, ftp://ftp-mouse.sanger.ac.uk]. "High-confidence" SNPs were defined by Sanger's criterion and denoted in the variant file by an above-threshold genotype (ATG) value = 1. There are additional variants in these genomes that will not be captured but the individualized genomes represent a good approximation to the actual genomes of these strains. SNPs and indels were incorporated into the reference mouse genome sequence (NCBIM37) to construct a strain-specific genome in fasta format. Genome coordinates in the gene annotation file (Ensembl version 67) were adjusted to reflect indels in each strain. The individualized genome and gene annotation files were used to construct strain-specific transcriptomes containing all annotated gene isoforms with SNPs and indels incorporated.

Genomic DNA was extracted from each DO mouse and genotyped at 7664 SNPs on the Mouse Universal Genotyping Array ("MUGA", GeneSeek) (Welsh and McMillan 2012). Founder haplotypes were inferred from SNP probe intensities, using a hidden Markov model in the DOQTL R package (Broman *et al.* 2012; Gatti *et al.* 2014). At each SNP, the genotype with the highest posterior probability was recorded, and genotype state transitions were inferred at the physical midpoint between adjacent markers with differing genotypes. Individual chromosomes were phased to construct haplotypes by minimizing the number of recombination events consistent with the observed genotypes. Accurate long-range phasing is not critical for our purposes. For each DO sample, this process yields two genotype transition files [designated left ("L") and right ("R")] from which a pair of homologs is reconstructed. Chromosomal coordinates are mapped back to the reference genome (NCBIM37) to obtain annotation specific to each homolog. A diploid transcriptome is constructed with two copies of each transcript, one for each homolog.

Seqnature uses the genotype transition files and founder strain variant call data to construct individualized genomes and gene annotation files. Seqnature scans through the variant call format (VCF) files, and at each position with a known SNP or indel, if the sample haplotype matches the founder strains with the variant, the variant is added to the individualized genome. For each sample two haploid genomes are produced and merged into one diploid genome file with chromosomes designated as L or R [*e.g.*, chromosome (Chr) 1L, Chr 1R]. Offset tracking data are used to update the coordinates of features in the gene annotation file (Ensembl v67), and the two annotation files are merged. The pair of records for each feature in the merged file is annotated to the L or R chromosomes and an additional annotation indicates the founder strain origin (A–H) of each feature. Features that span inferred recombination boundaries are labeled with both founders. One copy of the reference mitochondrial genome and any unassigned contig sequences are added to the merged genome sequence. One copy of the reference Y chromosome sequence is added to male samples.

Simulation of CAST and Diversity Outbred RNA-seq reads

We simulated RNA-seq reads from the CAST inbred strain and from a reconstructed DO individual, using the Flux Simulator (version 1.2) (Griebel *et al.* 2012). For each sample, we simulated 10 million and 30 million 100-bp single-end (CAST and DO) or paired-end (CAST only) reads with a standard error model (0.028% average mutations per sequence, 34.96 quality). For paired-end reads, we set the average fragment size at 280 with a standard deviation of 50, consistent with the fragment size distribution we observe in real Illumina RNA-seq data from current enzymatic fragmentation methods. Isoform abundance estimates derived from C57BL/6J liver RNA-seq data (aligned to the NCBIM37 reference) provide transcript abundance values for the FLUX parameter files. We simulated isoform abundance estimates for both alleles independently in the DO sample. We defined ground truth to be the realized abundance values obtained for the simulated RNA-seq reads. These will deviate somewhat from the input values due to simulated variation in the Flux library preparation and sequencing steps. The complete Flux parameter specifications are listed in Supporting Information, File S1.

For the eQTL simulations, we simulated 30 million 100-bp single-end reads from 277 DO genomes, using the rsem-simulate-reads command in RSEM [v1.2.8 (Li and Dewey 2011)]. We derived model files from abundance estimations on real DO samples (see the rsem-calculate-expression command and parameters described below) and used these values as initial input parameters for simulation. We set the fraction of reads that do not derive from any known transcript at the mean value of the proportion of unaligned reads observed in the real data ($\theta_0 = 0.018$).

Alignment of simulated and real RNA-seq reads to individualized transcriptomes

We used individualized transcriptomes to construct Bowtie-compatible indexes with the RSEM software (version 1.2.1) (Li and Dewey 2011). For inbred genomes (CAST and NCBIM37), each Ensembl transcript identifier (*e.g.*, ENSMUST00000000001) corresponds to a single sequence. For diploid genomes, each transcript identifier corresponds to two allelic sequences that are further differentiated with the L/R chromosome designation and their A–H founder strain designation (*e.g.*, ENSMUST00000000001FL and ENSMUST00000000001HR). The Bowtie aligner (version 0.12.8) (Langmead *et al.* 2009) aligns single-end reads, allowing up to three mismatches (-v 3), and only the best “strata” of alignments are reported. For a given read, the best stratum consists of the alignment(s) with the fewest mismatches. For paired-end reads, we set the maximum fragment size at 1000 (-X 1000) and used the -y option to maximize Bowtie’s sensitivity to find paired alignments.

Estimation of transcript abundance from read alignments

We obtained isoform- and gene-level abundance estimates with RSEM (version 1.2.1) (Li and Dewey 2011). RSEM executes an EM algorithm to compute a proportionate allocation of the reads with multiple alignments. RSEM estimates isoform-level abundance; gene-level abundance is calculated as the sum of the corresponding isoform counts. For diploid DO individuals, two allele-level abundance estimates are output for both isoforms and genes, and sample-level estimates are computed as the sum of alleles.

eQTL mapping

We obtained RNA-seq data from liver samples of 277 male and female DO mice fed a high-fat or standard chow diet. We mapped expression QTL, using gene-level counts estimated from alignment of reads to the reference NCBIM37 transcriptome and again using counts estimated from alignment to individualized transcriptomes. We applied the same processing and analysis steps to both sets of alignments. We included only genes with nonzero count values in ≥85% (≥233) of the DO samples in the eQTL analysis (17,125 genes from alignment to the NCBIM37 reference, 16,985 genes from alignment to individualized transcriptomes, and 16,924 genes in the common set). Raw counts in each sample were normalized to the upper quartile value and transformed to normal scores. We mapped expression QTL with DOQTL (Gatti *et al.* 2014), using a linear mixed model with sex, diet, sex by diet, and batch as additive covariates and a random polygenic term to account for genetic relatedness (Cheng *et al.* 2011).

We established significance thresholds by performing 100,000 permutations and fitting an extreme value distribution to the maximum logarithm of the odds ratio (LOD) scores (Dudbridge and Koeleman 2004). We converted permutation-derived *P*-values to *q*-values with the QVALUE software, using the bootstrap method to estimate π_0 and the default λ tuning parameters (Storey *et al.* 2004). We set the significance threshold for declaring an eQTL at a false discovery rate of 1% (Chesler *et al.* 2005).

Results

Construction of individualized genomes for RNA-seq read alignment

The DO is an outbred population derived from eight inbred mouse strains (Svenson *et al.* 2012). The seven nonreference founder strains of the DO population (A/J, 129S1/SvImJ, NOD/ShiLtJ, NZO/HlLtJ, CAST/EiJ, PWK/PhJ, and WSB/EiJ) differ from the reference strain C57BL/6J genomic sequence (NCBIM37) at a large number of loci (Table 1). Variation is especially high in the three wild-derived strains (CAST, PWK, and WSB). SNPs in the CAST transcriptome relative to the NCBIM37 reference occur at a rate of 1/217 bases and indels are present at 1/1650 bases. Thus half of all 100-bp reads from CAST should contain at least one SNP or indel.

The homologous chromosome pairs of a DO animal are each composed of a unique mosaic of founder strain haplotypes with several hundred recombination events. We used high-density genotyping and applied a hidden Markov model to estimate the phased haplotypes of each DO chromosome (Gatti *et al.* 2014) and placed haplotype transitions at the physical midpoint between the two flanking markers at each inferred recombination event. Intragenic transitions were rare; we observed 118 intragenic events of 75,124 total events, corresponding to 0.16% of recombination events in a typical DO genome. We create an individualized diploid genome by

Table 1 Annotated SNPs and indels segregating among the eight CC/DO founder strains

	Genome			Transcriptome		
Strain	SNPs	Insertions	Deletions	SNPs	Insertions	Deletions
A/J	4,198,324	401,264	422,424	104,358	7,846	8,394
129S1/SvImJ	4,458,004	428,081	458,055	109,598	8,154	8,875
NOD/ShiLtJ	4,323,530	389,285	407,801	108,881	7,599	8,168
NZO/HlLtJ	4,492,372	396,393	410,118	108,026	7,551	7,905
CAST/EiJ	17,673,726	1,359,607	1,367,482	410,805	26,975	27,474
PWK/PhJ	17,202,436	1,247,627	1,388,258	411,647	25,226	27,842
WSB/EiJ	6,045,573	588,061	608,945	146,495	10,966	11,559
All strains	31,593,523	2,963,385	3,213,340	746,993	56,354	61,204

For each of the founder strains, the cumulative numbers of high-quality SNPs, insertions, and deletions that differ from the NCBIM37 genome and transcriptome are listed. Transcript boundaries are based on the Ensembl v67 annotation. The bottom row tabulates the total number of variants segregating among the founder strains that differ from NCBIM37.

introducing known variants—SNPs and small indels—into two copies of the NCBIM37 reference genome. We use gene and isoform annotations (Ensembl version 67) to extract a diploid transcriptome, which will serve as the target for alignment of RNA-seq reads for the individual DO animal (Figure 1).

Performance on simulated data

We used simulated data to evaluate the accuracy of read alignment and transcript abundance estimation. We simulated 10 million 100-bp single-end reads from CAST and from a reconstructed DO genome, using the Flux Simulator (0.028% average mutations per sequence, 34.96 average quality) (Griebel *et al.* 2012). We aligned the simulated reads to NCBIM37 and to the individualized CAST and DO transcriptomes, allowing for three or fewer mismatches in the alignment algorithm. We compared the alignment of each read to its simulated origin and summarized results at the gene and isoform levels. We compared gene- and isoform-level abundance estimates from RSEM to the realized values from the simulated read set aligned using both stringent (zero mismatches allowed) and more relaxed (three or fewer mismatches allowed) alignment criteria.

At the gene level, a read can (i) align uniquely to the correct location; (ii) align to multiple locations, one of which is correct; (iii) fail to align to any locus with three or fewer mismatches; (iv) align to multiple locations, none of which are correct; or (v) align uniquely to the incorrect location. Categories are ordered from best to worst outcome. When comparing two alignment methods, we consider the number of reads that improve in these categories and the degree of improvement.

CAST alignment

We aligned 9,999,923 simulated CAST reads to each of the NCBIM37 and CAST transcriptomes and assessed gene-level alignment quality by the above criteria (Table 2). A total of 458,297 reads improve by alignment to the CAST transcriptome (Table 2, italic entries), of which 93% (427,016 of 458,297 reads) improve by two or more categories (Table 2, underlined italic entries). In comparison, only 10,533 reads improve by alignment to NCBIM37 (Table 2, entries in boldface type) of which only 3% (326 of 10,533 reads) improve by two or more categories (Table 2, entries in underlined boldface type). Isoform-level alignment is also improved by alignment to CAST. The frequency of multiple alignments at the isoform level is increased because many reads align to shared exons in multiple isoforms of a gene (Table S1).

Read alignment errors occur most frequently in genes with polymorphisms between CAST and NCBIM37, especially in genes with closely related gene family members or retrotransposed pseudogenes. The 3643 reads that align uniquely to the correct location in CAST but to an incorrect unique location in NCBIM37 (Table 2) originate from 163 genes and incorrectly align to 168 other genes (Table S2). These alignment errors occur between pairs or small sets of gene family members. For example, 1119 simulated reads from *Mug1* (murinoglobulin 1) align uniquely but incorrectly in NCBIM37 to the family member *Mug2* (murinoglobulin 2). Genes with retrotransposed pseudogenes are similarly sensitive to misalignment. For example, 130 reads from the protein-coding gene *Vcp* (valosin-containing protein) align uniquely but incorrectly in NCBIM37 to the pseudogene *Vcp-rs* (valosin-containing protein, related sequence). This extreme class of alignment error can cause major deviations in gene abundance estimates. In the case of *Vcp-rs*, the pseudogene is mistakenly classified as an expressed transcript. We also examined 405,895 reads that failed to align to NCBIM37 but are rescued to the unique, correct locus in CAST. These reads derive from nearly 10,000 genes (9599 genes with ≥1 reads; 4601 genes with ≥10 reads). Expression estimates for these genes are underestimated by alignment to NCBIM37.

CAST abundance estimates

Alignment of simulated CAST reads to the CAST transcriptome improves the accuracy of gene-level abundance estimation compared to alignment to NCBIM37 (Table 3). We restricted our analysis to genes for which either the ground truth or the estimated count was at least 10, yielding 12,186 genes after alignment to NCBIM37 and 12,108 after alignment to CAST. Highly accurate abundance

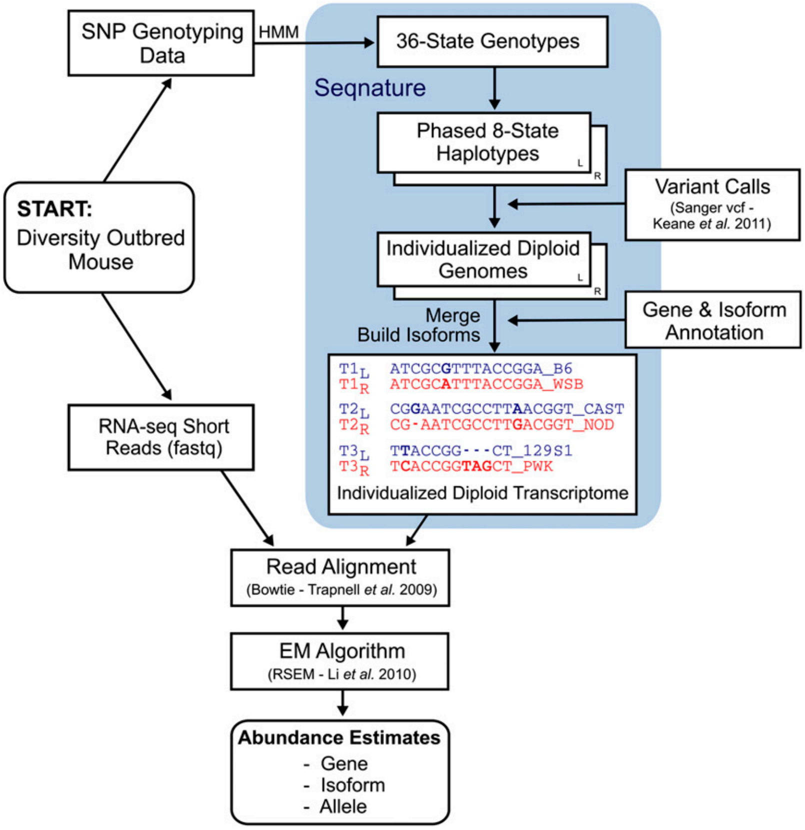

Figure 1 Flowchart showing the RNA-seq analysis pipeline and Seqnature tool. A Diversity Outbred mouse sample is shown as an example. Genomic DNA is genotyped at 7664 SNPs, which are then input into a hidden Markov model to impute 36-state founder strain genotypes. Seqnature (highlighted in blue) infers genotype transitions by calculating the smallest number of recombinations necessary to produce the observed 36-state patterns and outputs two 8-state genotype transition files. Seqnature constructs two haploid genomes by incorporating founder strain SNPs and indels into the reference genome according to the genotype transition files and creates two gene annotation files with adjusted coordinates (to offset insertions and deletions) and founder strain appended to feature identifiers. The two genomes and annotation files are merged, and then individualized diploid isoform sequences (individualized transcriptome) are constructed and indexed. Sample RNA-seq data are aligned with Bowtie to the individualized transcriptome, and allele-, isoform-, and gene-level abundances are estimated using an EM algorithm (RSEM) to resolve multimapped reads.

estimates—those within 5% of ground truth—occur for 4319 genes (35%) after alignment to NCBIM37 and for 8718 genes (72%) after alignment to CAST. A total of 8217 genes (67%) have gene-level abundance estimates within 10% of the ground truth after alignment to NCBIM37, compared to 10,544 (87%) of gene-level abundance estimates from alignment to CAST. There are 174 gene-level abundance estimates that differ by >50% from ground truth for the CAST alignment, *vs.* 485 such estimates after alignment to NCBIM37. If we consider only perfect-matching reads (reads that align with zero mismatches), only 24% of gene estimates from the NCBIM37 alignment are within 10% of ground truth compared to 79% of gene estimates from the CAST alignment. Increasing the read depth does not affect these conclusions (Table S3).

Diversity Outbred alignment

We aligned 9,999,338 simulated reads from a reconstructed DO genome to each of the NCBIM37 and individualized DO transcriptomes (Table 2). A total of 186,248 reads improve by alignment to the DO transcriptome (Table 2, italic entries) and most (146,083) improve by two or more categories (Table 2, underlined italic entries). In comparison, only 5384 reads improve by alignment to NCBIM37 (Table 2, entries in boldface type) and only 77 improve by two or more categories (Table 2, entries in underlined boldface type). As with CAST simulated reads, polymorphic genes with closely related gene family members or retrotransposed pseudogenes are most sensitive to read alignment errors. A total of 5618 reads from 73 genes align to the correct unique location in the individualized DO transcriptome but align uniquely to 79 other genes in NCBIM37. Another 137,938 reads from 5759 genes fail to align to NCBIM37 but align uniquely to the correct gene in the individualized transcriptome (Table S4).

Diversity Outbred abundance estimates

Alignment of DO reads to the individualized diploid DO transcriptome improves estimates of gene abundance (Table 3). We restricted our analysis to genes with ground truth or estimated counts of at least 10, yielding 11,899 genes after alignment to NCBIM37 and 11,863 genes after alignment to the individualized DO transcriptome. Highly accurate abundance estimates—those within 5% of ground truth—occur for 7260 genes (61%) after alignment to NCBIM37 and for 8569 genes (72%) after alignment to the individualized DO transcriptome. A total of 9805 genes (82%) have gene-level abundance estimates within 10% of the ground truth value after alignment to NCBIM37, compared to 10,471 (88%) of gene-level abundance estimates from alignment to the individualized DO transcriptome. There are 161 gene-level abundance estimates that differ by >50% from ground truth for the individualized DO alignment, *vs.* 230 such estimates after alignment to NCBIM37. If we consider only perfect-matching reads, only 40% of gene abundance estimates from alignment to NCBIM37 are within 10% of ground truth, compared to 81% of gene estimates from alignment

Table 2 Summary of read alignment in the simulated CAST and DO data

		Aligned to CAST					
CAST gene-level summary	Read class	Incorrect unique reads	Incorrect multireads	Unmapped reads	Correct multireads	Correct unique reads	Total
Aligned to NCBIM37	Incorrect unique reads	1,076	*0*	*4*	*11,225*	*3,643*	15,948
	Incorrect multireads	**0**	531	*0*	*5,145*	*1,104*	6,780
	Unmapped reads	**13**	**1**	1,709,356	*8,332*	*405,895*	2,123,597
	Correct multireads	**15**	**4**	**6**	976,821	*22,949*	999,795
	Correct unique reads	**3**	**0**	**291**	**10,200**	6,843,309	6,853,803
	Total	1,107	536	1,709,657	1,011,723	7,276,900	9,999,923

		Aligned to DO					
DO gene-level summary	Read class	Incorrect unique reads	Incorrect multireads	Unmapped reads	Correct multireads	Correct unique reads	Total
Aligned to NCBIM37	Incorrect unique reads	799	*1*	*7*	*3,675*	*1,136*	5,618
	Incorrect multireads	**0**	367	*0*	*2,732*	*595*	3,694
	Unmapped reads	**1**	**0**	1,712,660	*3,796*	*137,938*	1,854,395
	Correct multireads	**13**	**0**	**2**	865,550	*36,368*	901,933
	Correct unique reads	**1**	**0**	**62**	**5,305**	7,228,330	7,233,698
	Total	814	368	1,712,731	881,058	7,404,367	9,999,338

The simulated reads were aligned to the NCBIM37 and individualized transcriptomes, and alignments were collapsed to the genomic location. Reads that improve by alignment to the individualized transcriptomes are in italics, with those that improve by two or more categories in underlined italics. Reads that improve by alignment to NCBIM37 are in boldface type, with those that improve by two or more categories in underlined boldface type. Reads on the diagonal align equivalently by both strategies.

to the individualized DO transcriptome. Increasing the read depth does not affect these conclusions (Table S5).

Allele-specific expression

Alignment to an individualized diploid transcriptome provides direct estimates of allele-specific expression. We use the same EM algorithm that resolves genomic and isoform multireads to resolve allelic multireads. We analyzed the simulated DO data and compared the allele-specific count estimates to the ground truth. We restricted our analysis to the 5270 genes that were robustly expressed (total count ≥100) and had at least five aligned reads that overlapped one or more polymorphisms that distinguished the two alleles. Estimates of allele frequency, the proportion of reads assigned to the L allele in the DO simulation, are strongly correlated with ground truth ($r = 0.82$), with a median deviation of 4% (Figure 2). A small number of genes deviate considerably from ground truth. This is most evident for extreme estimates of allelic imbalance, which appear as horizontal lines of dots at the top and bottom of Figure 2. These errors may result from one or both of two scenarios. In the first scenario, they may expose a weakness of the EM algorithm. Even when the total read count is high, if the number of reads that distinguish the two alleles is low, the likelihood of sampling reads from only one of the alleles by chance can be substantial. In such cases, the EM algorithm will assign all reads to the allele with the unique read alignments. Bayesian analysis with an informative prior or introduction of pseudocounts could be implemented to correct this problem, but these methods will require further study. In the second scenario one or more allele-specific strain SNPs in these genes reduce the mappability of that particular allele and cause reads overlapping that SNP to align with less precision to multiple places in the genome. Increasing read depth to 30 million reads and increasing stringency of filtering to require a minimum of 10 unique allelic alignments reduces this problem (Figure S1), arguing against widespread mappability artifacts. Our diploid alignment strategy uses all unique allele read alignments within a gene to inform estimates of allele-specific expression, thus mitigating potential mappability artifacts stemming from any single variant.

Performance on real data

Individualized alignment of liver RNA-seq data from CAST and DO samples yields alignment statistics that are similar to our simulation results; this suggests that improvements in mapping accuracy and gene abundance estimates are also similar to the simulation results. We find that 75% of CAST reads align to the NCBIM37 transcriptome with three or fewer mismatches while 2.1% more reads (+252,905) align to the CAST transcriptome (Table S6). The difference between alignments is more striking for perfectly mapping reads (zero mismatch), as 23% more CAST reads (+982,229) align perfectly to CAST but not to NCBIM37. One-quarter of expressed genes in the CAST liver sample (2984 of 11,964 genes) yield gene-level abundance estimates that differ by >10% between alignment to the CAST and NCBIM37 transcriptomes (Figure 3A). For most of this cohort (2242 of 2984 genes) the simulation results show that the CAST alignment abundance estimates are closer to the ground truth (green circles in Figure 3A). This suggests that simulations can identify the genes that are most sensitive to choice of alignment target; the median difference between NCBIM37- and CAST-derived abundance estimates was 20% in the real data and 12% in the simulated data (green bars in Figure 3B). A set of 439 genes has

Table 3 Comparison of gene abundance estimates for simulated CAST and DO RNA-seq data after alignment to NCBIM37 reference and individualized transcriptomes

			No. genes with estimates *x*% from ground truth			
Aligned to	Mismatches allowed	Genes above threshold	<5%	<10%	>10%	>50%
CAST reads						
NCBIM37	3	12,186	4,319	8,217 (67)	3,969 (33)	485
CAST	3	12,108	8,718	10,544 (87)	1,542 (13)	174
NCBIM37	0	12,137	1,465	2,925 (24)	9,212 (76)	1,576
CAST	0	12,059	7,023	9,568 (79)	2,491 (21)	152
DO reads						
NCBIM37	3	11,899	7,260	9,805 (82)	2,094 (18)	230
DO IRG	3	11,863	8,569	10,471 (88)	1,380 (12)	161
NCBIM37	0	11,879	2,309	4,810 (40)	7,069 (60)	530
DO IRG	0	11,857	7,110	9,575 (81)	2,262 (19)	164

Alignment of simulated CAST reads to the individualized CAST transcriptome results in twice as many gene estimates ($N = +4399$) that fall within 5% of ground-truth value and fewer than half as many gene estimates ($N = -2427$) that deviate >10% from the ground truth. Gene estimates in the simulated DO sample are also improved by read alignment to the individualized transcriptome, yielding 18% more estimates ($N = +1309$) within 5% of the ground-truth value and 34% fewer estimates ($N = -714$) that deviate >10% from the ground truth.

abundance estimates that differ by >10% in the real data and showed an improvement over alignment to NCBIM37 in the simulation results (439 of 2984 genes) and the difference in abundance estimates between alignments is less variable. The median difference between NCBIM37- and CAST-derived abundance estimates was 16% in the real data and 5% in the simulated data (red circles and bars in Figure 3, A and B). Moreover, this suggests that the simulation study underestimated the actual differences in gene-level abundance estimates between alignment strategies, at least for the set of 2984 genes whose abundance estimates differ by >10% between alignment strategies in the real liver data.

Individualized alignment also improves read alignment accuracy and abundance estimates in the DO sample. We observed that 1% more reads (+151,225) align with three or fewer mismatches and 9% more reads (+704,522) align perfectly in the individualized DO transcriptome compared to NCBIM37 (Table S6). In the comparison of gene abundance estimates, we find that a total of 714 expressed genes differ by >10% from alignment strategy alone, and most of these (432 of 714 genes) show more accurate estimates from individualized alignment in the simulation study (green circles in Figure 3C). These genes appear to be highly sensitive to alignment strategy; the median difference in abundance estimates between NCBIM37 and individualized alignments was 16% in the real data and 14% in the simulated data (green bars in Figure 3D). Abundance estimates for 124 genes (124 of 714 genes) differ by >10% between alignment strategies in the real data and show an improvement from alignment to NCBIM37 in the simulation study (red circles in Figure 3C). The difference in gene abundance estimates between alignment strategies is less variable (median difference: 15%, real data; 5%, simulation study) (red bars in Figure 3D). Again, the simulation study appears to underestimate the actual differences in gene-level abundance estimates between alignment strategies.

Overall, the improvements in read alignment and gene-level abundance estimation are more modest in the DO sample relative to the CAST sample. This was expected given that five of the DO founder strains are closely related laboratory strains with greater similarity to the NCBIM37 reference compared to wild-derived strains such as CAST. That said, each DO sample will have a unique set of SNPs and indels that can bias read alignment, and in total across a large population of DO mice, the number of alignment-sensitive genes will approach the sum of all genes that are sensitive to alignment bias across all of the eight founder strains.

Individualized alignment reduces errors in RNA-seq eQTL studies

eQTL mapping on simulated data: We examined the effect of choice of alignment target on the identification of eQTL. We simulated 30 million single-end RNA-seq reads from each of 277 DO genomes and then mapped eQTL from the realized gene-level abundance values. In the simulated data, 15,027 genes pass the minimum coverage. Of these, 7033 have significant eQTL (6437 local and 596 distant eQTL) while 7994 genes have no significant eQTL at a false discovery rate (FDR) of 1%. Next, we aligned the simulated reads to the GRCm38 reference transcriptome and to the individualized diploid DO transcriptomes and compared the eQTL results mapped with the gene-level abundance estimates derived from these two strategies. Alignment of simulated reads to individualized DO transcriptomes yields a 98.3% accuracy rate in assigning eQTL—14,778 of 15,027 total calls are correct—and the 249 incorrect assignments are equally likely to be false negative or false positive associations (Table 4). In contrast, alignment of reads to the reference transcriptome results in 10% fewer correct assignments—only 13,250 of 15,027 total calls are correct—and most incorrect assignments result in false positive eQTL. Protein-coding genes are the predominant gene biotype in the simulated data set and as such account for most of the eQTL call improvements observed from the individualized alignment strategy (Table S7). Alignment to individualized transcriptomes improves eQTL call accuracy for all gene biotypes that exhibit eQTL

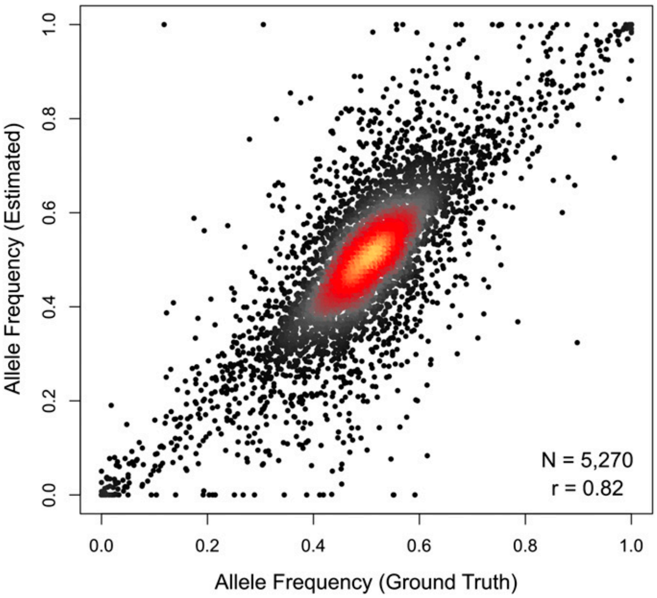

Figure 2 Read alignment to an individualized diploid transcriptome yields accurate allelic abundance estimates. Estimated allele frequency (*y*-axis) is plotted against the ground-truth allele frequency (*x*-axis) for 5270 genes in the simulated data set of 10 million DO reads that were robustly expressed (sum of allele counts ≥100) and had at least 5 uniquely aligned reads that differentiated the two gene alleles. Allele-level gene abundances are strongly correlated to the ground-truth values (*r* = 0.82), with the estimated frequency of the lower-expressed allele differing on average by <7% (median = 4%) from the ground-truth value. Most genes have a ground truth and estimated allele frequency near 0.5 (red and orange regions), and some estimates show absolute allele-specific expression (*i.e.*, 0 or 1) while the ground truth is somewhere in between (horizontal lines of dots at top and bottom).

differences from alignment strategy in the simulation; pseudogenes in particular are sensitive to false positive distant eQTL when aligned to the reference transcriptome (see explanation below). A comprehensive summary of the eQTL simulation results can be found in Table S8.

eQTL mapping on real data: We compared eQTL mapping on real liver RNA-seq data from 277 DO mice aligned to the NCBIM37 reference and to individualized DO transcriptomes. We identified significant local eQTL for 53% of expressed genes (8997 of 16,985 genes expressed above threshold; FDR = 1%) after alignment to individualized transcriptomes. Only 40% of expressed genes (6797 of 17,125 genes; FDR = 1%) had significant local eQTL after alignment to NCBIM37. For 2900 genes, a local eQTL is revealed only after alignment to individualized transcriptomes (Figure 4A). Among the 6097 local eQTL that are identified by both alignment strategies, most increase in significance from individualized alignments (Figure 4B). Individualized alignment improves the mapping resolution of local eQTL. Half of the 8997 significant local eQTL map within 372 kb of the midpoint of the gene they control (Table S9), compared to 428 kb for the 6767 local eQTL mapped in the NCBIM37 alignment (Table S10).

Significant distant eQTL are less common than strong local associations, accounting for 12% of the total eQTL (n = 931/7698; FDR = 1%) from alignment to NCBIM37 (Table S9) and 9% of total eQTL (n = 887/9884; FDR = 1%) from alignment to individualized transcriptomes (Table S10). Moreover, we find that many of the most highly significant distant eQTL are spurious and arise from alignment errors in NCBIM37. For example, after alignment to NCBIM37, expression of the pseudogene *Rps12-ps2* (located on Chr 14) appears to be controlled by a distant regulator on Chr 10 at the location of the *Rps12* protein coding gene (Figure 4C). DO animals that are CAST or PWK in the Chr 10 eQTL region exhibit apparently higher expression of *Rps12-ps2* (Figure S2A). Alignment of DO samples to individualized transcriptomes eliminates the distant eQTL for *Rps12-ps2* (Figure 4C and Figure S2B) and also eliminates a local eQTL peak at *Rps12* that showed a mirror-image pattern of allele effects. CAST- and PWK-derived reads in the individualized transcriptome align to the parent gene *Rps12* rather than to the retrotransposed pseudogene *Rps12-ps2*.

Concordance between inferred founder allele effects in the DO and observed expression patterns in the founder strains provides additional evidence in support of local eQTL. RNA-seq was performed on 128 male liver samples from the eight DO founder strains. We aligned reads to strain-specific transcriptomes and estimated gene-level abundance, following the same procedure as above. For example, the long noncoding RNA (lincRNA) Gm12976 is associated with a local eQTL on Chr 4 and with a distant eQTL on Chr 3 only after alignment to individualized transcriptomes (Figure 5A). DO animals with the chromosome 4 region derived from the 129S1/SvImJ founder strain show higher expression of Gm12976 (Figure 5A, inset). Allele-specific estimates of gene expression demonstrate that this local eQTL is acting in *cis* through expression of 129S1-derived alleles in the DO animals (Figure 5B). We observed this same pattern of expression in the eight founder strains (Figure 5C), and we observe high concordance overall between expression in the founder strains and founder allele estimates in the DO for genes with significant local eQTL (Figure S3).

Discussion

RNA-seq is a robust and highly informative technology; however, the increase in information content comes with increased analytical complexity. We have demonstrated that alignment of RNA-seq reads to a reference genome can result in biased transcript abundance estimates, much in the same way that a reference-based probe design can bias hybridization of genetically diverse samples to microarrays (Walter *et al.* 2007). Mismatch tolerance in the alignment algorithm can increase the number of reads that align in the presence of sequencing errors or genetic variation. However, error tolerance will also increase the frequency of misalignment to gene family members and pseudogenes. This problem is amplified in genetically diverse multiparent populations like the outbred DO stock and inbred Collaborative Cross (CC) strains. We have experimented with many different alignment

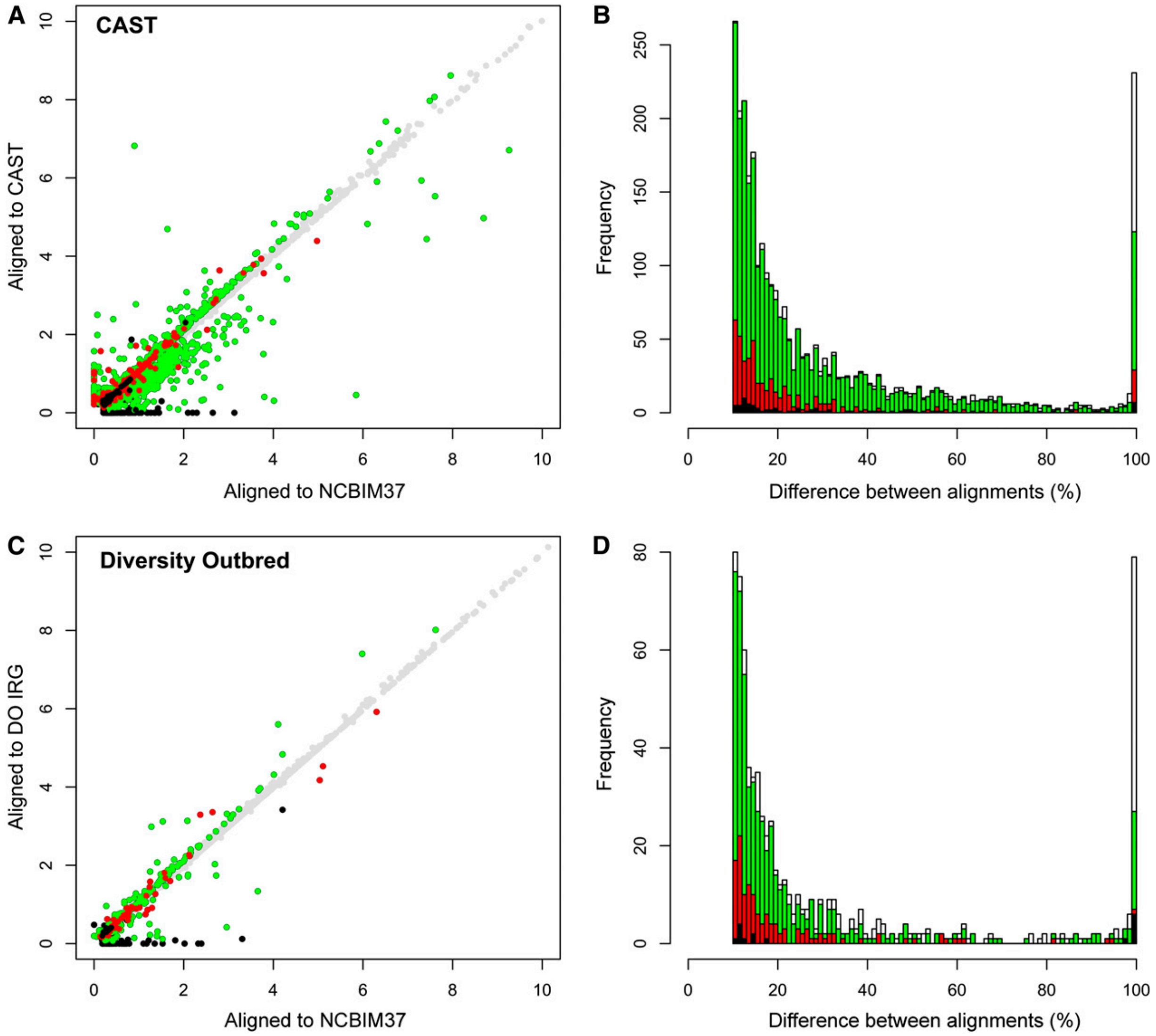

Figure 3 Gene-level abundance estimates in real data are improved by the individualized alignment strategy. (A) Gene-level abundance estimates are plotted for one CAST sample after alignment to the NCBIM37 (*x*-axis) and CAST transcriptomes (*y*-axis). Points are colored based on the difference between alignments and the results of the simulation study (*n* = 11,964 total genes). Gray circles denote genes with abundance estimates that differ by <10% between alignment strategies (*n* = 8980). Green denotes genes that differ in the real data by >10% between alignment strategies and for which the alignment to CAST improved the abundance estimate in the simulation study (*n* = 2242). Red denotes genes that differ by >10% in the real data and for which alignment to NCBIM37 improved the abundance estimate in the simulation study (*n* = 439). Black denotes genes that differ by >10% in the real data but for which the two alignment strategies yielded the same abundance estimates in the simulation study (*n* = 71). (B) The differences in gene-level abundance estimates between alignment strategies in the real CAST data are plotted as a stacked histogram. The percentage of difference between CAST and NCBIM37 alignments is plotted on the *x*-axis, and the total number of genes with that difference is plotted on the *y*-axis. The same coloring conventions are used as in A. White bars denote genes that differ by >10% in the real data but that were not expressed above threshold in the simulated data set (*n* = 232). Differences were scaled to a maximum value of 100%. (C) Gene-level abundance estimates are plotted for one DO sample after read alignment to the NCBIM37 (*x*-axis) and individualized transcriptomes (*y*-axis). A total of 714 genes in the real data differ by >10% between alignment strategies (*n* = 714/12,248), of which 432 gene estimates were improved by alignment to the individualized transcriptome in the simulation study (green circles), 124 were improved by alignment to NCBIM37 in the simulation (red circles), and 16 yielded the same gene estimate by both alignment strategies in the simulation study (black circles). (D) The difference in gene-level abundance estimates between alignment strategies in the real DO data are plotted as a stacked histogram. The percentage of difference between DO and NCBIM37 alignment is plotted on the *x*-axis, and the total number of genes with that difference is plotted on the *y*-axis. The same coloring conventions are used as in C. White bars denote genes that differ by >10% in the real data but that were not expressed above threshold in the simulation study (*n* = 142).

tools and consistently found the same problems in our eQTL mapping. While some alignment problems remain, the introduction of individual genome sequences corrects the majority of obvious anomalies and reveals a surprising amount of genetic regulatory information that was masked by alignment to the reference sequence.

Our knowledge of the genomes of the DO founder strains, especially the wild-derived strains, remains incomplete. These genomes were assembled by alignment of short DNA sequence reads to the mouse reference genome as a first step in identifying SNPs, indels, and structural variants (Keane *et al.* 2011). However, comprehensive elucidation of these genomes encompassing copy number variation and large-scale rearrangements will require *de novo* assembly from longer reads/ fragments (*e.g.*, mate pair sequences) and optical mapping. Similarly, we lack a comprehensive understanding of differences in transcription and splicing among these strains. In this study we restricted our focus to the reference set of Ensembl gene annotations largely derived from B6, with the understanding that this may not reflect some of the most important differences between highly diverse founder strains. We find evidence for this inadequacy by comparing the alignment summary statistics for B6 and CAST liver samples aligned to their respective strain-specific transcriptomes. Compared to CAST, more B6 reads align with fewer mismatches to fewer positions in the transcriptome, resulting in increased alignment specificity. A similar number of reads from CAST yield nearly twice as many valid alignments, and relaxing the aligner settings does not correct this problem (data not shown). We developed Seqnature software and the associated analysis pipeline as a first step toward maximizing the power and utility of sequencing technologies in multiparent mapping populations. As we learn more about the structure of the founder genomes and transcriptomes, this knowledge can be incorporated to produce more accurate representations of the individual transcriptomes sampled in our study. Alignment to individualized genomes presents a challenge for comparison and visualization of sample alignments; however, new tools make conversion back to reference genome coordinates straightforward (Huang *et al.* 2013).

For many genes, estimates of transcript abundance are relatively unaffected by alignment strategy. For example, 75% of expressed genes in CAST (n = 8980/ 11,964) have gene abundance estimates that differ by <10% after alignment to NCBIM37 and CAST, and most (n = 6855/ 11,964) differ by <5%. The subset of genes most sensitive to alignment method in real data consists primarily of closely related gene families and protein-coding genes with retrotransposed pseudogenes. Our simulations confirmed that pseudogenes can act as "read sinks" that shunt significant numbers of reads away from the protein-coding parent gene. Pseudogenes have long been considered functionless evolutionary relics; however, recent evidence suggests that some are actively transcribed and play critical roles in gene regulation (Zheng and Gerstein 2007; Muro *et al.* 2011; Poliseno 2012). There is not a clear delineation among gene, gene family, and pseudogene, and we feel that it is better to obtain accurate read alignments than to mask regions of low genomic mappability in the reference or apply a *post hoc* filtering based on gene annotations. After an individual's genetic variation is included in the alignment, particularly in the parent gene, many of these reads will align uniquely to the parent gene and be weighted accordingly by the EM algorithm (Figure S4 and Figure S5).

Table 4 Comparison of gene expression QTL (eQTL) from simulated DO RNA-seq data aligned to individualized or GRCm38 reference transcriptome

Assignment	Aligned to individualized	Aligned to GRCm38
Correct assignment		
Local eQTL (n = 6,437)	6,349	5,973
Distant eQTL (n = 596)	540	438
No eQTL (n = 7,994)	7,889	6,839
Total correct (%)	14,778 (98.3)	13,250 (88.2)
Incorrect assignment		
False negative	128	508
False positive, local	64	1,086
False positive, distant	57	183
Total incorrect (%)	249 (1.7)	1,777 (11.8)

Thirty million 100-bp RNA-seq reads were simulated from 277 DO genomes. eQTL mapping on the simulated gene expression values yields 7033 significant associations, including 6437 local and 596 distant eQTL, as well 7994 genes with no significant eQTL. Alignment of simulated DO reads to individualized transcriptomes improves the accuracy of eQTL mapping relative to alignment to GRCm38.

We have demonstrated that alignment to an individualized transcriptome is required to obtain accurate estimates of gene-level abundance when RNA is sequenced in genetically diverse samples. Many studies attempt to bypass this requirement by aligning reads to a common reference and discarding reads that do not align to a unique location (Lappalainen *et al.* 2013; Battle *et al.* 2014). However, it is clear from our analysis that many reads align uniquely in the individualized genome but align to multiple locations or fail to align to the reference genome—these highly informative reads would be discarded after alignment to the reference. Moreover, our results confirm published reports that relative gene abundance estimates based solely on unique read counts are biased—genes composed primarily of unique sequence are overestimated while genes with closely related pseudogenes or family members are underestimated (Mortazavi *et al.* 2008; Li and Dewey 2011). The inclusion of multireads adds complexity to the abundance estimation problem but EM algorithms are well suited to this task (Li and Dewey 2011; Nicolae *et al.* 2011; Turro *et al.* 2011; Roberts and Pachter 2013).

Read alignment to individualized transcriptomes improves estimation of isoform abundance; however, isoform-level resolution remains challenging due to splicing complexity, shared exon sequence, and the short length of reads from current sequencing platforms. Forty percent of mouse genes have multiple isoforms (n = 15,079/37,991 genes; median = 4 isoforms) that share substantial exon sequence. Most 100-bp reads align equally well to multiple gene isoforms and in the absence of unique isoform reads the EM algorithm cannot assign isoform reads to a single isoform with any confidence (Table S11). Paired-end sequencing produces modest improvements in isoform quantification (Table S12); however, in our experience current enzymatic fragmentation protocols yield fragments that are too short to provide a clear benefit from paired-end sequences. Longer fragments and reads will

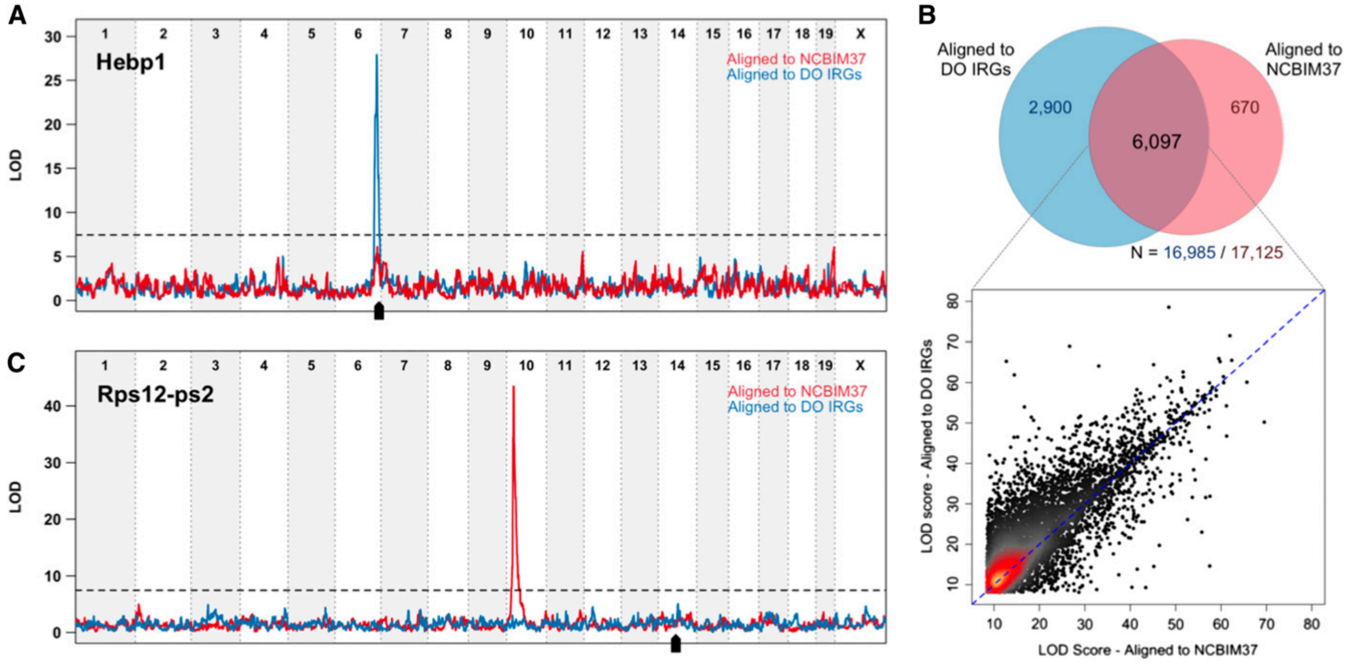

Figure 4 Alignment of Diversity Outbred mice to individualized transcriptomes (DO IRGs) reveals significant local eQTL and reduces the number of spurious pseudogene eQTL. (A) An example of a local eQTL unmasked by alignment to individualized transcriptomes. Expression estimates for *Hebp1* do not appear linked to local genotype when reads are aligned to the common reference (red line). Accounting for individual genetic variation in the alignment step uncovers a strong local eQTL with a peak centered at the gene (blue line; black arrow denotes gene location). (B) Venn diagram showing the overlap of local eQTL from the individualized or common reference alignment strategy. Local eQTL are identified for a majority of expressed genes by one or both alignment strategies. Alignment to individualized transcriptomes (DO IRGs) identifies 2900 novel local associations. Even in the case of the 6097 local eQTL that are identified as significant by both alignments (overlapping region), LOD significance scores are generally higher after alignment to individualized transcriptomes (*y*-axis in scatterplot) compared to NCBIM37 (*x*-axis). (C) Alignment to individualized transcriptomes reduces the number of spurious distant eQTL at pseudogenes. Accounting for segregating founder strain polymorphisms in the parent protein-coding gene *Rps12* ablates the distant Chr 10 eQTL peak for the pseudogene *Rps12-ps2* (compare blue to red lines) located on Chr 14.

improve isoform resolution in the future, but we found that summarization at the gene level with 100-bp single-end reads is robust.

Alignment to individualized transcriptomes yields new insights into gene regulation in multiparent populations. For example, by aligning reads from DO mice to a single search space that includes individualized sequences of both alleles for every annotated isoform, our analysis approach provides direct estimates of allele-specific expression. By simulation, we have shown that 10 unique allele-level read alignments provide enough specificity to accurately estimate allele-specific gene expression and that sequencing to a depth of 30 million is sufficient for 5000+ genes to meet this threshold in a DO sample. The Seqnature software and analysis approach can be applied to other next generation sequencing technologies such as Chip-seq to identify allelic differences in transcription factor occupancy (Reddy *et al.* 2012) or DNase I sensitivity mapping to identify allele-specific chromatin activation (Degner *et al.* 2012).

Previous eQTL studies in genetically diverse populations suggest that the most significant eQTL tend to be local (Rockman and Kruglyak 2006; Pickrell *et al.* 2010; Aylor *et al.* 2011; Lappalainen *et al.* 2013). Gene prioritization methods are becoming more important in the genome-wide association studies (GWAS) era (Hou and Zhao 2013), and genes with local eQTL are promising candidates for underlying disease-associated regions in human GWAS studies (Knight 2005; Chen *et al.* 2008; Emilsson *et al.* 2008; Musunuru *et al.* 2010; Hou and Zhao 2013; Li *et al.* 2013). An eQTL may arise from any of several biological mechanisms, including rate of transcription, rate of degradation, or processing of RNA intermediates. The eQTL reflects a difference in abundance of the transcript that is associated with a marker locus but does not necessarily identify the mechanism. We have shown with simulated and real RNA-seq data that incorporation of individual genetic variation at the alignment step is critical to all downstream analyses in high throughput sequencing studies including eQTL identification. Alignment of short sequence reads from genetically diverse individuals to a common reference, as has been done in most previous RNA-seq studies (Landt *et al.* 2012), will cause spurious eQTL associations and mask real associations. In our study, eQTL mapping with gene abundance estimates derived from read alignment to the reference transcriptome missed nearly 3000 significant local eQTL associations. Importantly, all sequencing applications will be sensitive to these alignment errors. Thus a causal variant that manifests as a local eQTL may be

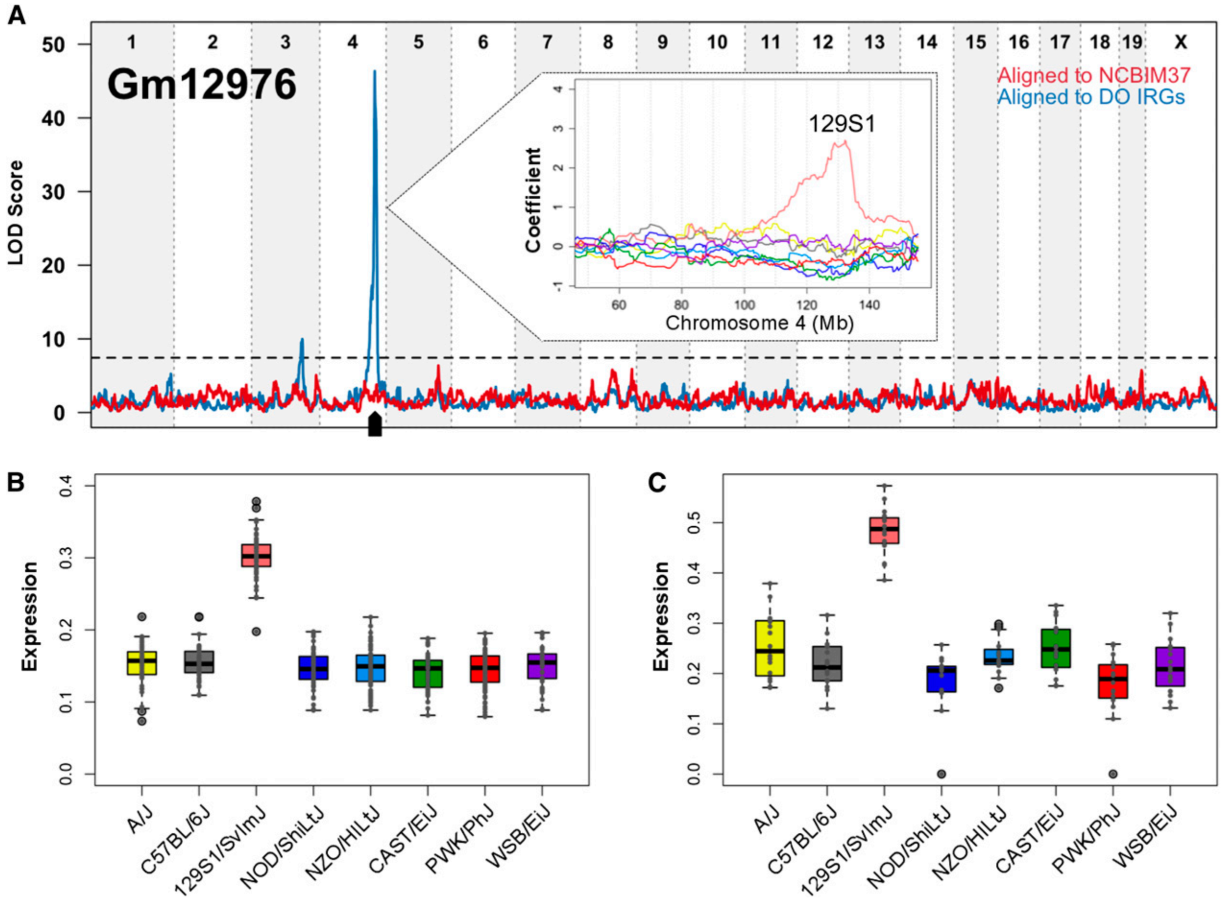

Figure 5 Liver expression patterns observed in the DO founder strains suggest that novel local eQTL are real. (A) Alignment to individualized transcriptomes (DO IRGs, blue line) reveals a strong local eQTL for the lincRNA Gm12976 on Chr 4. The eight founder strain coefficients inferred from the additive mapping model are plotted in the inset and show that DO animals that derive this region of Chr 4 from the 129S1/SvImJ strain have higher expression of Gm12976. (B) Allele-level abundance estimates in the DO population show that the 129S1 allele of Gm12976 is high expressing, confirming that the local eQTL is due to *cis*-acting variation. Founder strain origin is listed on the *x*-axis, and Gm12976 allelic abundance (upper quartile normalized, square-root transformed) is plotted on the *y*-axis. (C) This inferred DO strain pattern of Gm12976 expression is concordant with that observed in the eight founder strains. Strains are listed on the *x*-axis, and Gm12976 abundance (upper quartile normalized, square-root transformed) is plotted on the *y*-axis.

obscured by the common reference alignment approach. Gene prioritization strategies that utilize sequence data analyzed by the common reference approach will fail to identify these variants. Conversely, our simulation study shows that alignment errors to the reference transcriptome can sensitize a large group of genes to false positive local eQTL. In summary, failure to incorporate individual genetic variation at the alignment step will adversely affect read alignment and consequent analyses such as abundance estimation, eQTL identification, and eQTL fine-mapping. We have developed Seqnature and the associated analysis pipeline to be flexible with respect to species and type of sequencing application to support a broad array of experiments in genetically heterogeneous populations.

Data accession

Individualized genomes and annotation files for the DO founder strains A/J, 129S1/SvImJ, NOD/ShiLtJ, NZO/HlLtJ, CAST, PWK/PhJ, and WSB/EiJ, as well as the unmodified NCBIM37 (∼B6) reference genome and Ensembl v67 gene annotation files, are available for download at http://cgd.jax.org/tools/Seqnature.shtml. The Seqnature software for constructing individualized genomes and gene annotation files is available for download at https://github.com/jaxcs/Seqnature. Simulation data are available at http://cgd.jax.org/tools/Seqnature.shtml. Raw RNA-seq fastq files and processed gene-level data are archived at Gene Expression Omnibus under accession no. GSE45684.

Acknowledgments

S.C.M, N.R., K.C., J.H.G, M.A.H., E.J.C, and G.A.C. designed experiments; S.C.M., N.R., and K.C. performed experiments; S.C.M, N.R., K.C., D.M.G, J.H.G., E.J.C., and G.A.C. analyzed data; S.C.M., A.K.S., N.R., K.C., D.M.G., K.L.S., D.A.H., M.P.K., and A.D.A. contributed reagents/materials/analysis tools; and S.C.M and G.A.C. wrote the article with input from all authors. The authors declare no competing financial interests.

The authors thank L. Somes and M. Strobel for breeding the mice and S. Ciciotte, S. Daigle, S. Kamdar, J. Pereira, C. Snow, and R. Lynch for extracting RNA and performing RNA-seq experiments. Research reported here was supported by The Jackson Laboratory and National Institutes of Health (NIH) grants under awards P50GM076468 (to G.A.C.); DK091207, DK66369, and DK58037 (to A.D.A.); and F32HD074299 (to S.C.M.).

Literature Cited

Aylor, D. L., W. Valdar, W. Foulds-Mathes, R. J. Buus, R. A. Verdugo *et al.*, 2011 Genetic analysis of complex traits in the emerging Collaborative Cross. Genome Res. 21: 1213–1222.

Battle, A., S. Mostafavi, X. Zhu, J. B. Potash, M. M. Weissman *et al.*, 2014 Characterizing the genetic basis of transcriptome diversity through RNA-sequencing of 922 individuals. Genome Res. 24(1): 14–24.

Broman, K. W., 2012 Haplotype probabilities in advanced intercross populations. G3 **2:** 199–202.

Chen, Y., J. Zhu, P. Y. Lum, X. Yang, S. Pinto *et al.*, 2008 Variations in DNA elucidate molecular networks that cause disease. Nature 452: 429–435.

Cheng, R., M. Abney, A. A. Palmer, and A. D. Skol, 2011 QTLRel: an R package for genome-wide association studies in which relatedness is a concern. BMC Genet. 12: 66.

Chesler, E. J., L. Lu, S. Shou, Y. Qu, J. Gu *et al.*, 2005 Complex trait analysis of gene expression uncovers polygenic and pleiotropic networks that modulate nervous system function. Nat. Genet. 37(3): 233–242.

Churchill, G. A., D. M. Gatti, S. C. Munger, and K. L. Svenson, 2012 The Diversity Outbred mouse population. Mamm. Genome 23: 713–718.

Degner, J. F., J. C. Marioni, A. A. Pai, J. K. Pickrell, E. Nkadori *et al.*, 2009 Effect of read-mapping biases on detecting allele-specific expression from RNA-sequencing data. Bioinformatics 25: 3207–3212.

Degner, J. F., A. A. Pai, R. Pique-Regi, J. B. Veyrieras, D. J. Gaffney *et al.*, 2012 DNase I sensitivity QTLs are a major determinant of human expression variation. Nature 482(7385): 390–394.

Derrien, T., J. Estellé, S. M. Sola, D. G. Knowles, E. Raineri *et al.*, 2012 Fast computation and applications of genome mappability. PLoS ONE 7(1): e30377.

Dudbridge, F., and B. P. Koeleman, 2004 Efficient computation of significance levels for multiple associations in large studies of correlated data, including genomewide association studies. Am. J. Hum. Genet. 75: 424–435.

Emilsson, V., G. Thorleifsson, B. Zhang, A. S. Leonardson, F. Zink *et al.*, 2008 Genetics of gene expression and its effect on disease. Nature 452: 423–428.

Gatti, D. M., K.L. Svenson, A. Shabalin, L. Wu, W. Valdar *et al.*, 2014 Quantitative trait locus mapping methods for Diversity Outbred mice. G3 4: 1623–1633.

Graze, R. M., L. L. Novelo, V. Amin, J. M. Fear, G. Casella *et al.*, 2012 Allelic imbalance in Drosophila hybrid heads: exons, isoforms, and evolution. Mol. Biol. Evol. 29(6): 1521–1532.

Griebel, T., B. Zacher, P. Ribeca, E. Raineri, V. Lacroix *et al.*, 2012 Modelling and simulating generic RNA-Seq experiments with the flux simulator. Nucleic Acids Res. 40(20): 10073–10083.

Huang, S., C. Kao, L. McMillan, and W. Wang. 2013 Transforming genomes using MOD files with applications, *Proceedings of the International Conference on Bioinformatics, Computational Biology and Biomedical Informatics*. ACM, Washington, DC. Available at: http://www.cs.ucla.edu/~weiwang/paper/ACMBCB13_1.pdf.

Hou, L., and H. Zhao, 2013 A review of post-GWAS prioritization approaches. Front. Genet. 4: 280.

Keane, T. M., L. Goodstadt, P. Danecek, M. A. White, K. Wong *et al.*, 2011 Mouse genomic variation and its effect on phenotypes and gene regulation. Nature 477: 289–294.

Knight, J. C., 2005 Regulatory polymorphisms underlying complex disease traits. J. Mol. Med. 83: 97–109.

Landt, S. G., G. K. Marinov, A. Kundaje, P. Kheradpour, F. Pauli *et al.*, 2012 ChIP-seq guidelines and practices of the ENCODE and modENCODE consortia. Genome Res. 22: 1813–1831.

Langmead, B., C. Trapnell, M. Pop, and S. L. Salzberg, 2009 Ultrafast and memory-efficient alignment of short DNA sequences to the human genome. Genome Biol. 10: R25.

Lappalainen, T., M. Sammeth, M. R. Friedlander, P. A. C. ‘t Hoen, J. Monlong *et al.*, 2013 Transcriptome and genome sequencing uncovers functional variation in humans. Nature 501: 506–511.

Li, B., and C. Dewey, 2011 RSEM: accurate transcript quantification from RNA-Seq data with or without a reference genome. BMC Bioinformatics 12(1): 323.

Li, B., V. Ruotti, R. M. Stewart, J. A. Thomson, and C. N. Dewey, 2010 RNA-Seq gene expression estimation with read mapping uncertainty. Bioinformatics 26: 493–500.

Li, H., and R. Durbin, 2009 Fast and accurate short read alignment with Burrows-Wheeler transform. Bioinformatics 25(14): 1754–1760.

Li, Q., J. H. Seo, B. Stranger, A. McKenna, I. Pe’er *et al.*, 2013 Integrative eQTL-based analyses reveal the biology of breast cancer risk loci. Cell 152: 633–641.

Lister, R., R. C. O’Malley, J. Tonti-Filippini, B. D. Gregory, C. C. Berry *et al.*, 2008 Highly integrated single-base resolution maps of the epigenome in *Arabidopsis*. Cell 133(3): 523–536.

McKenna, A., M. Hanna, E. Banks, A. Sivachenko, K. Cibulskis *et al.*, 2010 The Genome Analysis Toolkit: a MapReduce framework for analyzing next-generation DNA sequencing data. Genome Res. 20: 1297–1303.

McManus, C. J., J. D. Coolon, M. O. Duff, J. Eipper-Mains, B. R. Graveley *et al.*, 2010 Regulatory divergence in Drosophila revealed by mRNA-seq. Genome Res. 20(6): 816–825.

Mortazavi, A., B. A. Williams, K. McCue, L. Schaeffer, and B. Wold, 2008 Mapping and quantifying mammalian transcriptomes by RNA-Seq. Nat. Methods 5: 621–628.

Mouse Genome Sequencing Consortium, 2002 Initial sequencing and comparative analysis of the mouse genome. Nature 420: 520–562.

Muro, E. M., N. Mah, and M. A. Andrade-Navarro, 2011 Functional evidence of post-transcriptional regulation by pseudogenes. Biochimie 93: 1916–1921.

Musunuru, K., A. Strong, M. Frank-Kamenetsky, N. E. Lee, T. Ahfeldt *et al.*, 2010 From noncoding variant to phenotype via SORT1 at the 1p13 cholesterol locus. Nature 466: 714–719.

Nagalakshmi, U., Z. Wang, K. Waern, C. Shou, D. Raha *et al.*, 2008 The transcriptional landscape of the yeast genome defined by RNA sequencing. Science 320: 1344–1349.

Nicolae, M., S. Mangul, I. I. Măndoiu, and A. Zelikovsky, 2011 Estimation of alternative splicing isoform frequencies from RNA-Seq data. Algorithms Mol. Biol. 6(1): 9.

Patro, R., S. M. Mount, and C. Kingsford, 2014 Sailfish enables alignment-free isoform quantification from RNA-seq reads using lightweight algorithms. Nat. Biotechnol. 32: 462–464.

Pickrell, J. K., J. C. Marioni, A. A. Pai, J. F. Degner, B. E. Engelhardt *et al.*, 2010 Understanding mechanisms underlying human gene expression variation with RNA sequencing. Nature 464 (7289): 768–772.

Poliseno, L., 2012 Pseudogenes: newly discovered players in human cancer. Sci. Signal. 5: re5.

Reddy, T. E., J. Gertz, F. Pauli, K. S. Kucera, K. E. Varley *et al.*, 2012 Effects of sequence variation on differential allelic transcription factor occupancy and gene expression. Genome Res. 22(5): 860–869.

Rivas-Astroza, M., D. Xie, X. Cao, and S. Zhong, 2011 Mapping personal functional data to personal genomes. Bioinformatics 27(24): 3427–3429.

Roberts, A., and L. Pachter, 2013 Streaming fragment assignment for real-time analysis of sequencing experiments. Nat. Methods 10(1): 71–73.

Rockman, M. V., and L. Kruglyak, 2006 Genetics of global gene expression. Nat. Rev. Genet. 7: 862–872.

Rozowsky, J., A. Abyzov, J. Wang, P. Alves, D. Raha *et al.*, 2011 AlleleSeq: analysis of allele-specific expression and binding in a network framework. Mol. Syst. Biol. 7: 522.

Satya, R. V., N. Zavaljevski, and J. Reifman, 2012 A new strategy to reduce allelic bias in RNA-Seq readmapping. Nucleic Acids Res. 40: e127.

Shen, Y., T. Garcia, V. Pabuwal, M. Boswell, A. Pasquali *et al.*, 2013 Alternative strategies for development of a reference transcriptome for quantification of allele specific expression in organisms having sparse genomic resources. Comp. Biochem. Physiol. Part D Genomics Proteomics 8(1): 11–16.

Skelly, D. A., M. Johansson, J. Madeoy, J. Wakefield, and J. M. Akey, 2011 A powerful and flexible statistical framework for testing hypotheses of allele-specific gene expression from RNA-seq data. Genome Res. 21(10): 1728–1737.

Stevenson, K. R., J. D. Coolon, and P. J. Wittkopp, 2013 Sources of bias in measures of allele-specific expression derived from RNA-seq data aligned to a single reference genome. BMC Genomics 14: 536.

Storey, J. D., J. E. Taylor, and D. Seigmund, 2004 Strong control, conservative point estimation and simultaneous conservative consistency of false discovery rates: a unified approach. J. R. Stat. Soc. B 66(Part 1): 187–205.

Svenson, K. L., D. M. Gatti, W. Valdar, C. E. Welsh, R. Cheng *et al.*, 2012 High-resolution genetic mapping using the Mouse Diversity outbred population. Genetics 190: 437–447.

Trapnell, C., L. Pachter, and S. L. Salzberg, 2009 TopHat: discovering splice junctions with RNA-Seq. Bioinformatics 25(9): 1105–1111.

Trapnell, C., B. A. Williams, G. Pertea, A. Mortazavi, G. Kwan *et al.*, 2010 Transcript assembly and quantification by RNA-Seq reveals unannotated transcripts and isoform switching during cell differentiation. Nat. Biotechnol. 28(5): 511–515.

Turro, E., S. Y. Su, A. Goncalves, L. J. Coin, S. Richardson *et al.*, 2011 Haplotype and isoform specific expression estimation using multi-mapping RNA-seq reads. Genome Biol. 12: R13.

Walter, N. A., S. K. McWeeney, S. T. Peters, J. K. Belknap, R. Hitzemann *et al.*, 2007 SNPs matter: impact on detection of differential expression. Nat. Methods 4: 679–680.

Wang, Z., M. Gerstein, and M. Snyder, 2009 RNA-Seq: a revolutionary tool for transcriptomics. Nat. Rev. Genet. 10: 57–63.

Welsh, C. E., and L. McMillan, 2012 Accelerating the inbreeding of multi-parental recombinant inbred lines generated by sibling matings. G3 **2:** 191–198.

Wu, T. D., and S. Nacu, 2010 Fast and SNP-tolerant detection of complex variants and splicing in short reads. Bioinformatics 26(7): 873–881.

Zheng, D., and M. B. Gerstein, 2007 The ambiguous boundary between genes and pseudogenes: The dead rise up, or do they? Trends Genet. 23: 219–224.

Communicating editor: S. F. Chenoweth

GENETICS

Supporting Information
http://www.genetics.org/lookup/suppl/doi:10.1534/genetics.114.165886/-/DC1

RNA-Seq Alignment to Individualized Genomes Improves Transcript Abundance Estimates in Multiparent Populations

Steven C. Munger, Narayanan Raghupathy, Kwangbom Choi, Allen K. Simons, Daniel M. Gatti, Douglas A. Hinerfeld, Karen L. Svenson, Mark P. Keller, Alan D. Attie, Matthew A. Hibbs, Joel H. Graber, Elissa J. Chesler, and Gary A. Churchill

DOI: 10.1534/genetics.114.165886

File S1

Supplemental Methods

Simulation parameters

RNA-seq reads were simulated from the CAST inbred strain and from a reconstructed DO individual using the Flux Simulator (version 1.2) and the parameters below.

Command line argument: flux-simulator –lsp Parameter_filename.txt

Single-end sequence parameters

```
REF_FILE_NAME      path/to/Gene_annotations.gtf
GEN_DIR            path/to/Genome.fa
LIB_FILE_NAME      filename.lib
SEQ_FILE_NAME      filename.bed
PRO_FILE_NAME      filename.pro
RT_PRIMER                    PDT
READ_NUMBER        10000000 (or 30000000)
READ_LENGTH        100
FILTERING                    true
SIZE_DISTRIBUTION   N(280,50)
FASTA              true
TSS_MEAN                     NaN
POLYA_SCALE        NaN
POLYA_SHAPE        NaN
ERR_FILE           76
```

Paired-end sequence parameters

```
REF_FILE_NAME      path/to/Gene_annotations.gtf
GEN_DIR            path/to/Genome.fa
LIB_FILE_NAME      filename.lib
SEQ_FILE_NAME      filename.bed
PRO_FILE_NAME      filename.pro
RT_PRIMER                    PDT
READ_NUMBER        60000000
READ_LENGTH        100
PAIRED_END                   YES
FILTERING                    true
SIZE_DISTRIBUTION   N(280,50)
FASTA              true
TSS_MEAN                     NaN
POLYA_SCALE        NaN
POLYA_SHAPE        NaN
ERR_FILE           76
```

Table S1 Isoform-level summary of read alignment in the simulated CAST data

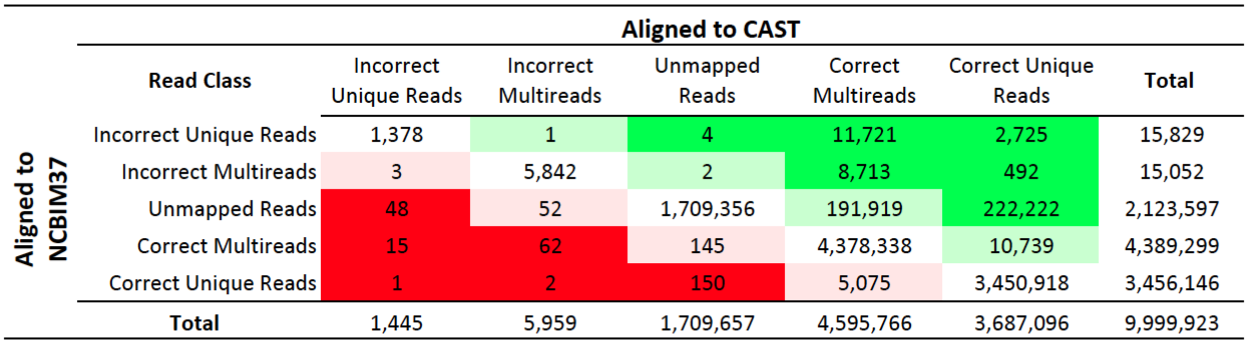

		Aligned to CAST					
	Read Class	Incorrect Unique Reads	Incorrect Multireads	Unmapped Reads	Correct Multireads	Correct Unique Reads	**Total**
Aligned to NCBIM37	Incorrect Unique Reads	1,378	1	4	11,721	2,725	15,829
	Incorrect Multireads	3	5,842	2	8,713	492	15,052
	Unmapped Reads	48	52	1,709,356	191,919	222,222	2,123,597
	Correct Multireads	15	62	145	4,378,338	10,739	4,389,299
	Correct Unique Reads	1	2	150	5,075	3,450,918	3,456,146
	Total	1,445	5,959	1,709,657	4,595,766	3,687,096	9,999,923

The simulated reads were aligned to the NCBIM37 and CAST transcriptomes. Reads that improve by alignment to CAST are highlighted in green, with those that improve by two or more categories are highlighted in dark green. Reads that improve by alignment to NCBIM37 are highlighted in red, with those that improve by two or more categories highlighted in dark red. Reads on the diagonal align equivalently by both strategies.

Table S2 List of genes from the CAST simulation that were affected by read misalignment or alignment failure from the reference alignment strategy

Three lists of genes are included in the attached table. The first list shows genes for which simulated CAST reads align uniquely but falsely in the NCBIM37 transcriptome. Alignment to the CAST transcriptome rescues these reads to their correct, unique origin (second list). The third list shows genes from which reads fail to align at all in the NCBIM37 transcriptome but align to the correct, unique position in the CAST transcriptome.

Table S2 is available for download as a MS Excel file at
http://www.genetics.org/lookup/suppl/doi:10.1534/genetics.114.165886/-/DC1

Table S3 Comparison of gene-level abundance results from alignment of 30 million simulated CAST reads to NCBIM37 and CAST transcriptomes

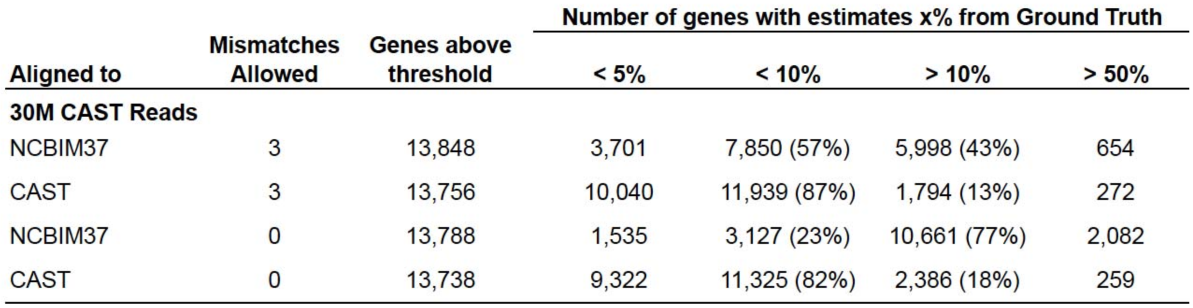

			Number of genes with estimates x% from Ground Truth			
Aligned to	**Mismatches Allowed**	**Genes above threshold**	**< 5%**	**< 10%**	**> 10%**	**> 50%**
30M CAST Reads						
NCBIM37	3	13,848	3,701	7,850 (57%)	5,998 (43%)	654
CAST	3	13,756	10,040	11,939 (87%)	1,794 (13%)	272
NCBIM37	0	13,788	1,535	3,127 (23%)	10,661 (77%)	2,082
CAST	0	13,738	9,322	11,325 (82%)	2,386 (18%)	259

Alignment of 30 million simulated CAST reads to the individualized CAST transcriptome (≤3 mismatches) results in nearly three times as many gene estimates (N= +6,339) that fall within 5% of ground truth value and fewer than a third as many gene estimates (N= -4,204) that deviate more than 10% from the ground truth. Gene-level abundance results for perfect matching reads (i.e. 0 mismatches) are also shown.

Table S4 List of genes from the DO simulation that were affected by read misalignment or alignment failure from the reference alignment strategy

Three lists of genes are included in the attached table. The first list shows genes for which simulated DO reads align uniquely but falsely in the NCBIM37 transcriptome. Alignment to the DO transcriptome rescues these reads to their correct, unique origin (second list). The third list shows genes from which reads fail to align at all in the NCBIM37 transcriptome but align to the correct, unique position in the DO transcriptome.

Table S4 is available for download as a MS Excel file at
http://www.genetics.org/lookup/suppl/doi:10.1534/genetics.114.165886/-/DC1

Table S5 Comparison of gene-level abundance results from alignment of 30 million simulated DO reads to NCBIM37 and individualized DO transcriptomes

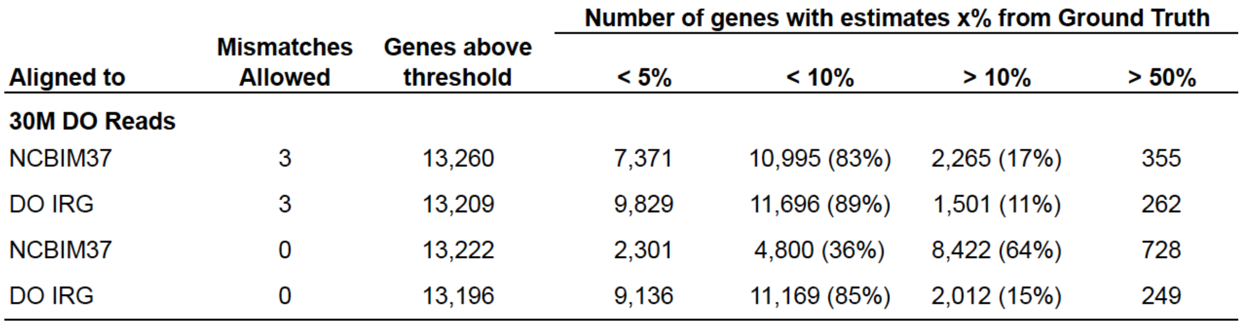

			Number of genes with estimates x% from Ground Truth			
Aligned to	Mismatches Allowed	Genes above threshold	< 5%	< 10%	> 10%	> 50%
30M DO Reads						
NCBIM37	3	13,260	7,371	10,995 (83%)	2,265 (17%)	355
DO IRG	3	13,209	9,829	11,696 (89%)	1,501 (11%)	262
NCBIM37	0	13,222	2,301	4,800 (36%)	8,422 (64%)	728
DO IRG	0	13,196	9,136	11,169 (85%)	2,012 (15%)	249

Gene estimates in the simulated DO sample are improved by read alignment to the individualized transcriptome (≤3 mismatches), yielding 33% more gene estimates (N= +2,458) within 5% of the ground truth value and 34% fewer estimates (N= -764) that deviate more than 10% from the ground truth. Gene-level abundance results for perfect matching reads (i.e. 0 mismatches) are also shown.

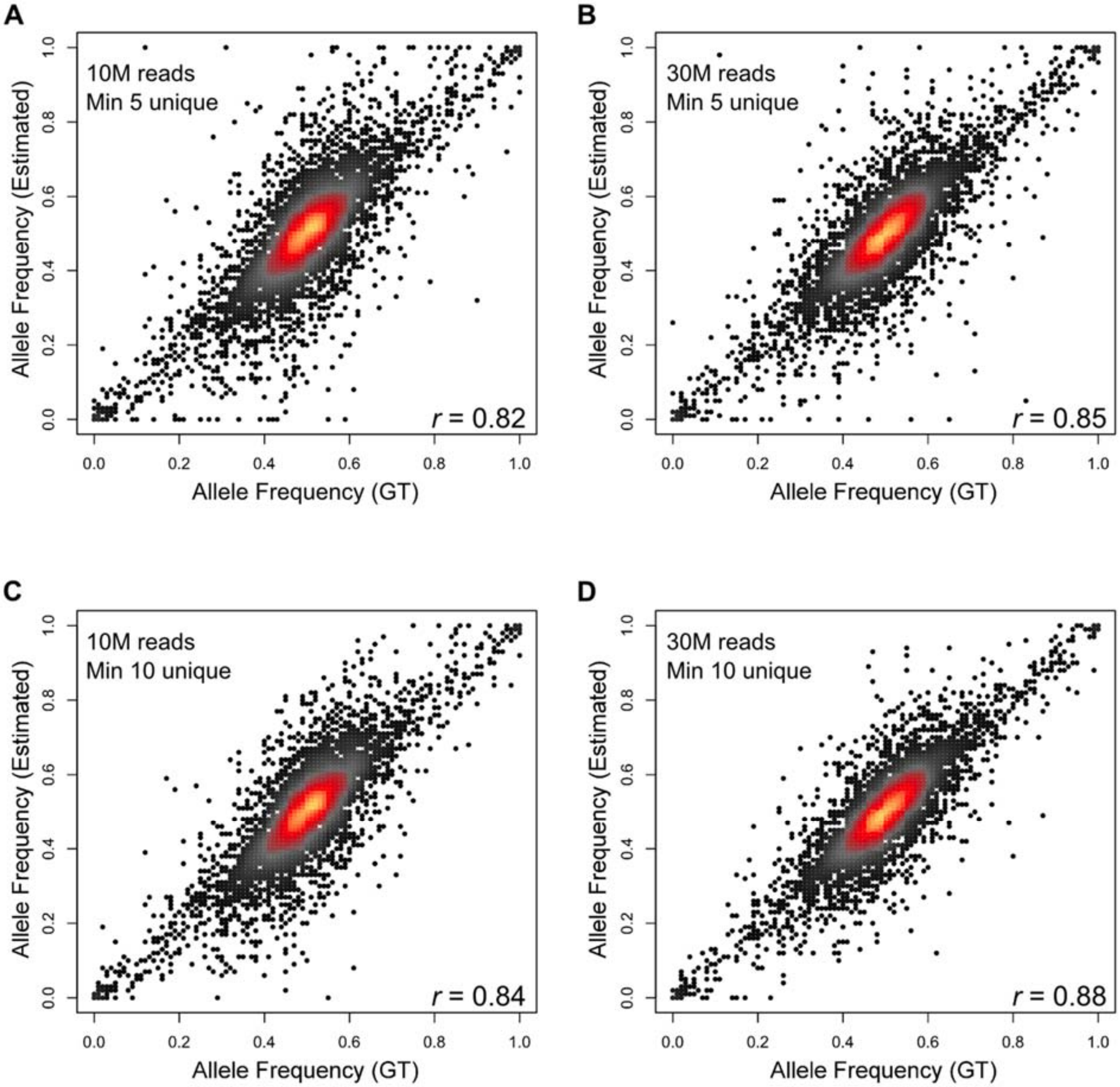

Figure S1 Characterization of sequencing depth and unique read threshold on estimation of allele-specific expression. Estimated allele frequency (y-axis) is plotted in panels A-D against the ground truth allele frequency (x-axis) for robustly expressed genes (sum of allele counts ≥ 100) in the simulated DO dataset. Allele frequency estimates are improved by increasing the read depth from 10 million (panels A and C) to 30 million reads (panels B and D) and by increasing the gene inclusion stringency to require ten (panels C and D) rather than five (panels A and B) reads with unique allele alignments.

Table S6 Alignment statistics for real CAST and DO liver RNA-seq data

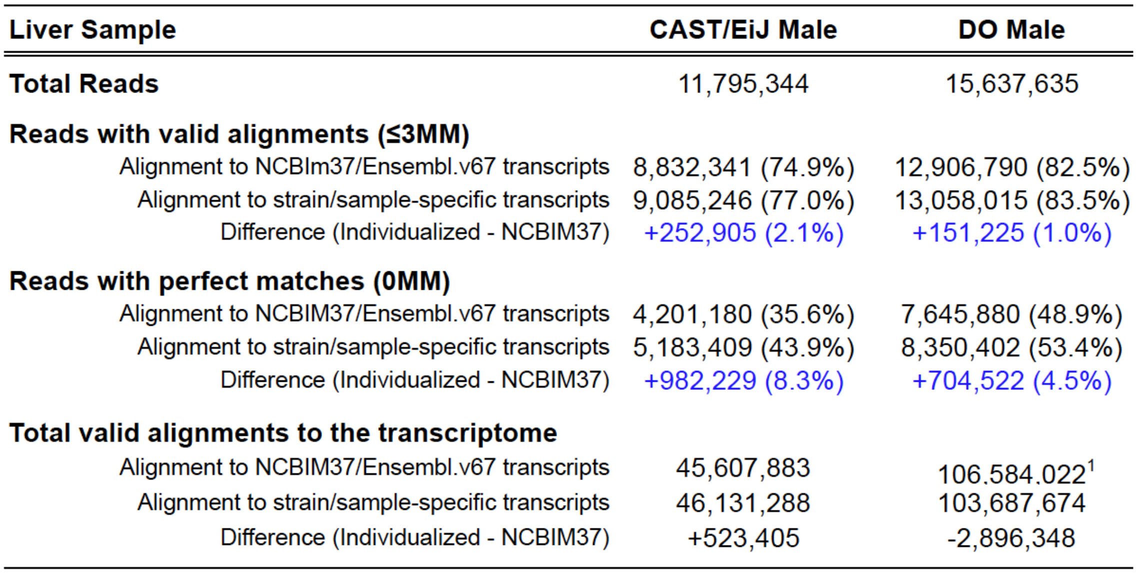

Liver Sample	CAST/EiJ Male	DO Male
Total Reads	11,795,344	15,637,635
Reads with valid alignments (≤3MM)		
Alignment to NCBIm37/Ensembl.v67 transcripts	8,832,341 (74.9%)	12,906,790 (82.5%)
Alignment to strain/sample-specific transcripts	9,085,246 (77.0%)	13,058,015 (83.5%)
Difference (Individualized - NCBIM37)	+252,905 (2.1%)	+151,225 (1.0%)
Reads with perfect matches (0MM)		
Alignment to NCBIM37/Ensembl.v67 transcripts	4,201,180 (35.6%)	7,645,880 (48.9%)
Alignment to strain/sample-specific transcripts	5,183,409 (43.9%)	8,350,402 (53.4%)
Difference (Individualized - NCBIM37)	+982,229 (8.3%)	+704,522 (4.5%)
Total valid alignments to the transcriptome		
Alignment to NCBIM37/Ensembl.v67 transcripts	45,607,883	106.584.022[1]
Alignment to strain/sample-specific transcripts	46,131,288	103,687,674
Difference (Individualized - NCBIM37)	+523,405	-2,896,348

Bowtie (version 0.12.8) parameters: -v 3 -a -m --best --strata

[1] For comparison to the diploid transcriptome alignments in DO samples, the total number of alignments to NCBIM37 were scaled by 2x.

Alignment of real data to individualized CAST- or DO-specific transcriptomes yields more reads with valid alignments (≤ 3 mismatches (MM)), and significantly more reads with perfect (0 MM) alignments. Reads align with greater specificity (i.e. fewer alignments per mapped read) to individualized transcriptomes than to NCBIM37.

Table S7 eQTL simulation summary showing the classification of eQTL calls that differ between alignment strategies differentiated by gene biotype

	Correct Calls			Incorrect Calls		
Gene Biotype	True Local	True Distant	True No eQTL	False Negative	False Positive Local	False Positive Distant
Antisense	2	3	15	-2	-16	-2
IG_C_gene	0	0	1	0	-1	0
lincRNA	6	3	15	-7	-15	-2
misc_RNA	2	0	2	-2	-1	-1
Mt_rRNA	0	0	0	0	0	0
non_coding	0	0	0	0	0	0
polymorphic pseudogene	1	0	0	-1	0	0
processed_transcript	3	0	2	-3	-2	0
protein_coding	336	94	981	-353	-980	-78
pseudogene	23	3	32	-10	-7	-41
retrotransposed	3	-1	1	-2	1	-2
sense_intronic	0	0	1	0	-1	0
sense_overlapping	0	0	0	0	0	0
snoRNA	0	0	0	0	0	0
Total	**376**	**102**	**1050**	**-380**	**-1022**	**-126**

Choice of read alignment strategy affects ten percent of genes (n = 1,528/15,027 total) in our simulation study. Alignment to individualized DO transcriptomes yields the correct eQTL assignment for all but one gene with a discordant call. Many gene biotypes yield incorrect eQTL calls after alignment to GRCm38 but pseudogenes in particular appear to be sensitive to false positive distant associations.

Table S8 Gene-level summary of eQTL simulation results

Columns 1-7 give information for the expressed gene, columns 8-10 show the SNP identifier and location for the marker with the highest LOD score in the simulation, and columns 11-13 provide details of the simulated eQTL including LOD score, p-value, and eQTL class (e.g., significant local or distant eQTL, no eQTL). Columns 14-19 show the eQTL mapping results after alignment of the simulated reads to the GRCm38 reference transcriptome. Column 18 shows the eQTL assignment relative to the simulated ground truth, and Column 19 lists whether the peak SNP associated with gene expression after alignment to GRCm38 matches the simulated peak SNP. Columns 20-25 show the same classes of eQTL data but after alignment of the simulated reads to individualized DO transcriptomes.

TableS8 is available for download as a MS Excel file at
http://www.genetics.org/lookup/suppl/doi:10.1534/genetics.114.165886/-/DC1

Table S9 List of eQTL from alignment to individualized DO transcriptomes

Columns 1-6 give information for the expressed gene, columns 7-9 show the SNP identifier and location for the marker with the highest LOD score, and columns 10-13 provide details of the eQTL including LOD score, raw p-value, adjusted q-value, and position relative to the controlled transcript (i.e. local or distal eQTL).

TableS9 is available for download as a tab-delimited text file at http://www.genetics.org/lookup/suppl/doi:10.1534/genetics.114.165886/-/DC1

Table S10 List of eQTL from alignment to NCBIM37

Columns 1-6 give information for the expressed gene, columns 7-9 show the SNP identifier and location for the marker with the highest LOD score, and columns 10-13 provide details of the eQTL including LOD score, raw p-value, adjusted q-value, and position relative to the controlled transcript (i.e. local or distal eQTL).

TableS10 is available for download as a tab-delimited text file at
http://www.genetics.org/lookup/suppl/doi:10.1534/genetics.114.165886/-/DC1

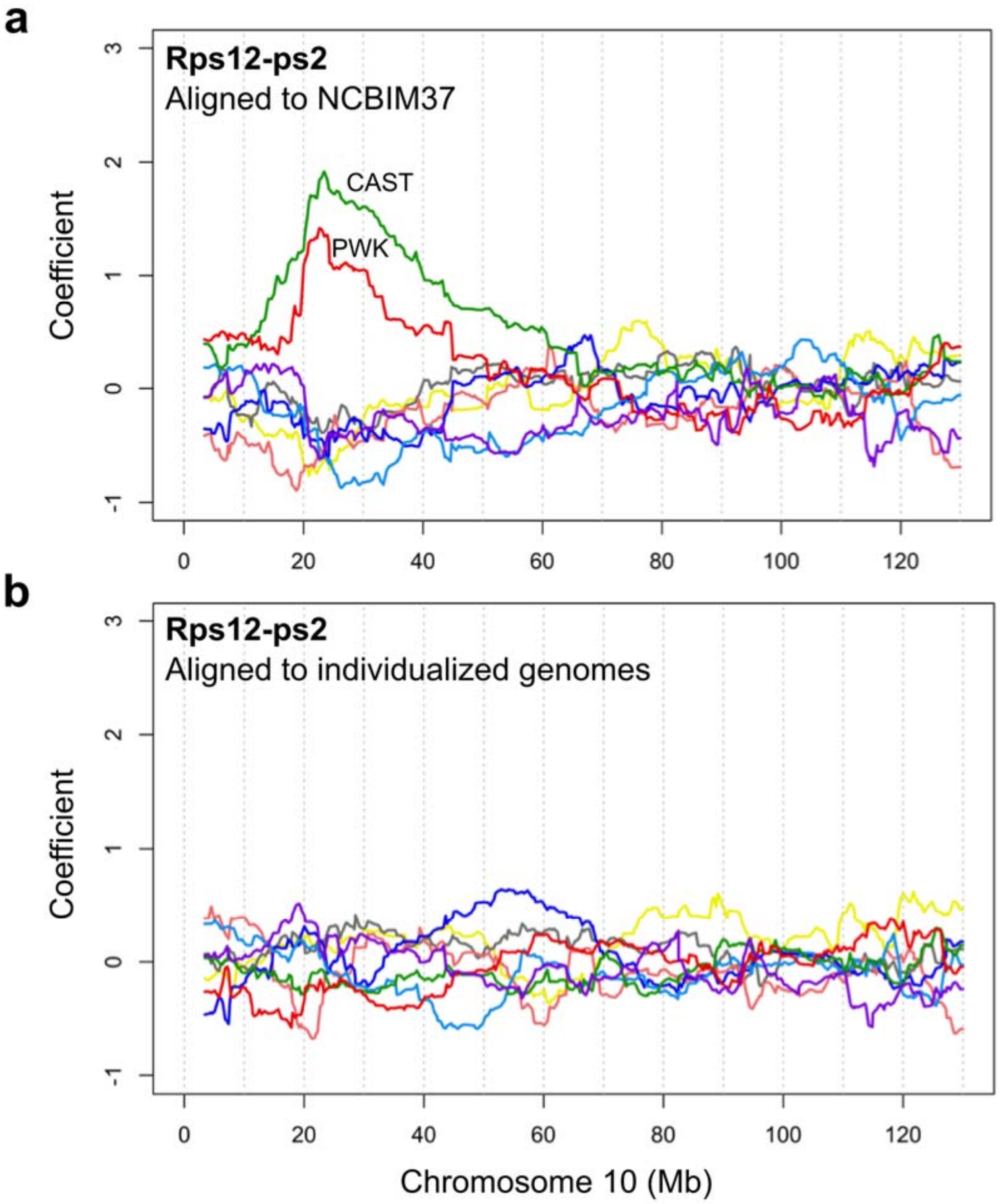

Figure S2 Comparison of Chromosome 10 founder coefficient plots for *Rps12-ps2* expression derived from alignment to NCBIM37 or individualized DO transcriptomes. Read alignment to individualized DO transcriptomes ameliorates spurious alignments to pseudogenes. When DO reads are aligned to the NCBIM37 reference transcriptome (A), it appears that DO animals that derive the Chr 10 region from CAST or PWK have higher expression of the pseudogene *Rps12-ps2*. When individual genetic variation is accounted for in the alignment (B), the CAST- and PWK-derived reads align preferentially to the parent protein coding gene *Rps12*, and the spurious *Rps12-ps2* eQTL is eliminated.

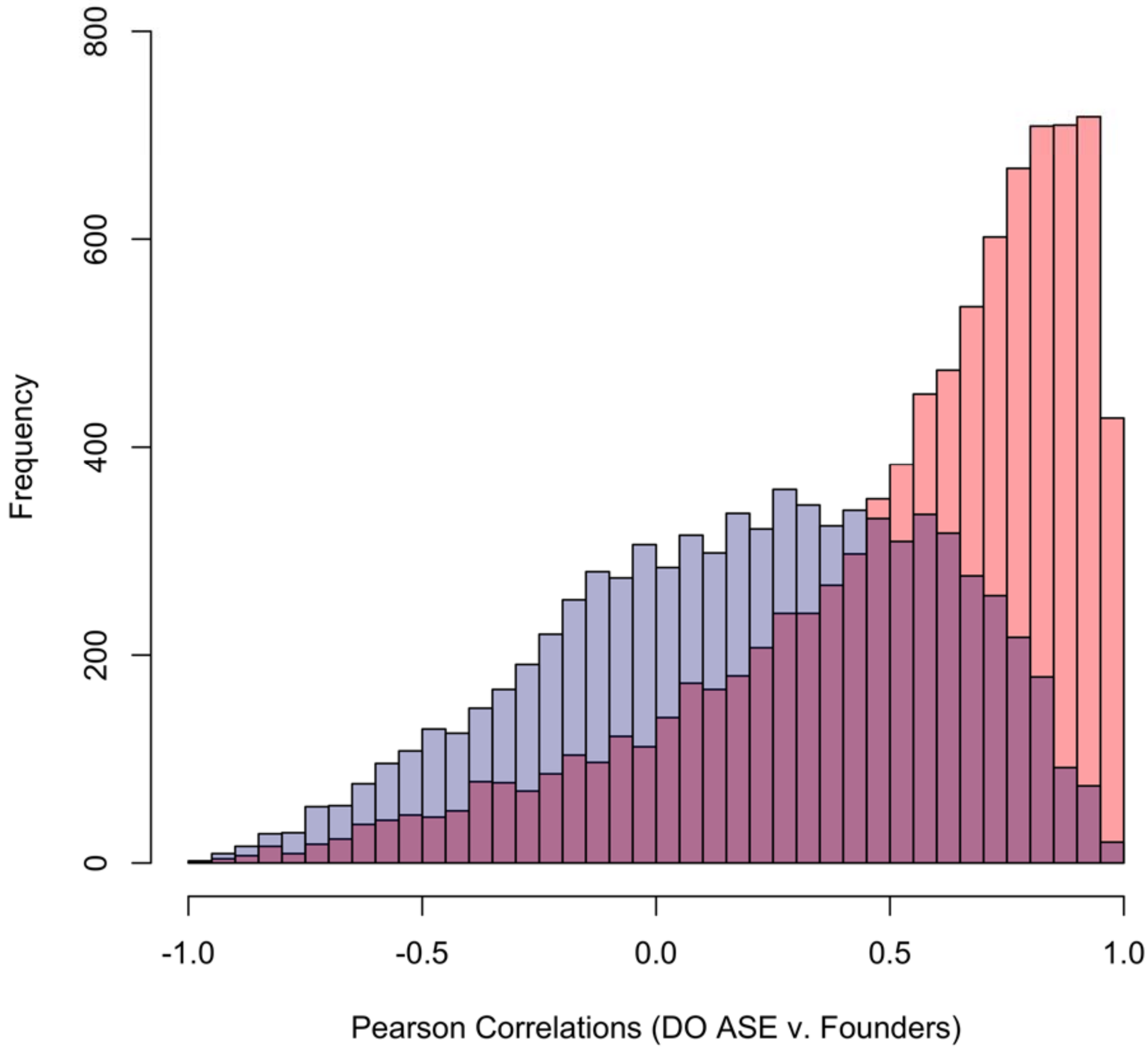

Figure S3 Comparison of gene-level expression in Founder strain samples and founder allele-level estimates in the DO samples for genes with and without significant local eQTL after alignment to individualized genomes. Pearson correlations between founder strain expression and founder allele estimates in the DO population are plotted as a histogram above. Founder allele estimates for genes with significant local eQTL (n=8,981 genes, shown in pink) exhibit higher concordance to gene-level liver expression in Founder strain samples compared to genes that do not have significant local eQTL (n=7,893 genes, shown in blue).

Table S11 Isoform abundance results in CAST simulation study

10 Million Simulated CAST reads

			Number of isoforms with estimates x% from Ground Truth			
Aligned to	**Mismatches Allowed**	**Isoforms above threshold**	**< 5%**	**< 10%**	**> 10%**	**> 50%**
NCBIM37	3	21,568	3,908	6,581 (30%)	14,987 (70%)	7,096
CAST	3	21,457	3,244	7,796 (36%)	13,661 (64%)	6,551
NCBIM37	0	21,363	1,393	2,883 (13%)	18,480 (87%)	9,488
CAST	0	21,222	1,998	5,089 (24%)	16,133 (76%)	6,540

30 Million Simulated CAST reads

			Number of isoforms with estimates x% from Ground Truth			
Aligned to	**Mismatches Allowed**	**Isoforms above threshold**	**< 5%**	**< 10%**	**> 10%**	**> 50%**
NCBIM37	3	27,048	3,600	7,217 (27%)	19,831 (73%)	9,821
CAST	3	26,910	6,685	9,951 (37%)	16,959 (63%)	9,031
NCBIM37	0	26,909	1,765	3,454 (13%)	23,455 (87%)	12,748
CAST	0	26,695	6,792	9,578 (36%)	17,013 (64%)	8,821

Alignment of simulated CAST reads to the individualized CAST transcriptome (≤3 mismatches) improves estimates of isoform abundance compared to alignment to NCBIM37. Increasing the sequencing depth from 10 to 30 million single-end reads significantly does not improve isoform resolution – more isoform estimates fall within five percent of the simulated ground truth but the total number of isoforms expressed above threshold increases too, causing no relative improvement in the accuracy of isoform abundance estimates. Isoform-level abundance results for perfect matching reads (i.e. 0 mismatches) are also shown.

Table S12 Comparison of isoform abundance results in CAST simulation study from using paired-end or single-end sequencing

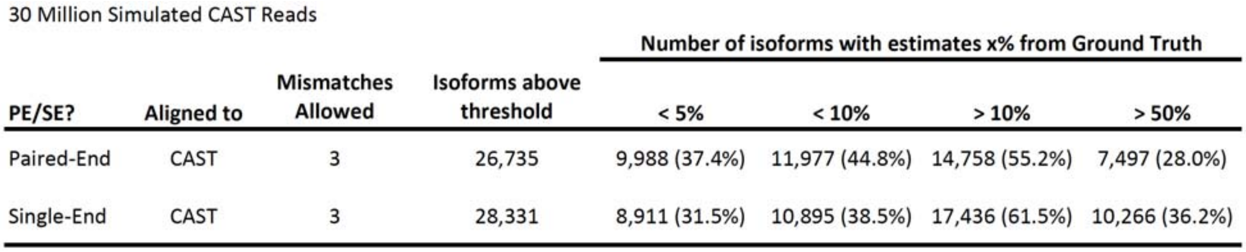

30 Million Simulated CAST Reads

PE/SE?	Aligned to	Mismatches Allowed	Isoforms above threshold	Number of isoforms with estimates x% from Ground Truth			
				< 5%	< 10%	> 10%	> 50%
Paired-End	CAST	3	26,735	9,988 (37.4%)	11,977 (44.8%)	14,758 (55.2%)	7,497 (28.0%)
Single-End	CAST	3	28,331	8,911 (31.5%)	10,895 (38.5%)	17,436 (61.5%)	10,266 (36.2%)

Paired-end sequencing yields modest improvements in isoform abundance estimation relative to single-end reads. For example, 45% of isoform estimates fall within ten percent of the simulated ground truth value in the analysis of paired-end reads, compared to 39% for single-end reads.

Figure S4

a

```
Ftl1-001_NCBIM37     1 AGGTCCCGTGGATCTGTGTCTTGCTTCAACAGTGTTTGAACGGAACAGACCCGGGGATTC
Ftl1-001_CAST        1 ............................................................
Ftl2-001_NCBIM37     1 ------------------------------------------------------------
Ftl2-001_CAST        1 ------------------------------------------------------------


Ftl1-001_NCBIM37    61 CCACTGTACTCGCTTCCAGCCGCCTTTACAAGTCTCTCCAGTCGCAGCCTCCGGGACCAT
Ftl1-001_CAST       61 ............................................................
Ftl2-001_NCBIM37     1 ------------------------------------------------------------
Ftl2-001_CAST        1 ------------------------------------------------------------


Ftl1-001_NCBIM37   121 CTCCTCGCTGCCTTCAGCTCCTAGGACCAGTCTGCACCGTCTCTTCGCGGTTAGCTCCTA
Ftl1-001_CAST      121 ...............G............................................
Ftl2-001_NCBIM37     1 ------------------------------------------------------------
Ftl2-001_CAST        1 ------------------------------------------------------------


Ftl1-001_NCBIM37   181 CTCCGGATCAGCCATGACCTCTCAGATTCGTCAGAATTATTCCACCGAGGTGGAAGCTGC
Ftl1-001_CAST      181 ............................................................
Ftl2-001_NCBIM37     1 -------------...............................................
Ftl2-001_CAST        1 -------------...............................................


Ftl1-001_NCBIM37   241 CGTGAACCGCCTGGTCAACTTGCACCTGCGGGCCTCCTACACCTACCTCTCTCTGGGCTT
Ftl1-001_CAST      241 ............................................................
Ftl2-001_NCBIM37    48 ............................................................
Ftl2-001_CAST       48 ............................................................


Ftl1-001_NCBIM37   301 CTTTTTTGATCGGGATGACGTGGCTCTGGAGGGCGTAGGCCACTTCTTCCGCGAATTGGC
Ftl1-001_CAST      301 ............................................................
Ftl2-001_NCBIM37   108 ............................................................
Ftl2-001_CAST      108 ............................................................


Ftl1-001_NCBIM37   361 CGAGGAGAAGCGCGAGGGCGCGGAGCGTCTCCTCGAGTTTCAGAACGATCGCGGGGGCCG
Ftl1-001_CAST      361 ............................................................
Ftl2-001_NCBIM37   168 ............................................................
Ftl2-001_CAST      168 ............................................................


Ftl1-001_NCBIM37   421 TGCACTCTTCCAGGATGTGCAGAAGCCATCTCAAGATGAATGGGGTAAAACCCAGGAGGC
Ftl1-001_CAST      421 ............................................................
Ftl2-001_NCBIM37   228 ............................................................
Ftl2-001_CAST      228 ............................................................
```

Figure S4 (continued)

```
                                         *
Ftl1-001_NCBIM37   481 CATGGAAGCTGCCTTGGCCATGGAGAAGAACCTGAATCAGGCCCTCTTGGATCTGCATGC
Ftl1-001_CAST      481 ...................T........................................
Ftl2-001_NCBIM37   288 ...................C........................................
Ftl2-001_CAST      288 ...................C........................................

                                        *
Ftl1-001_NCBIM37   541 CCTGGGTTCTGCCCGCGCGGACCCTCATCTCTGTGACTTCCTGGAAAGCCACTATCTGGA
Ftl1-001_CAST      541 ..................C.........................................
Ftl2-001_NCBIM37   348 ......C...........C..................................TC.....
Ftl2-001_CAST      348 ......C...........C..................................TC.....


Ftl1-001_NCBIM37   601 TAAGGAGGTGAAACTCATCAAGAAGATGGGCAACCATCTGACCAACCTCCGCAGGGTGGC
Ftl1-001_CAST      601 ............................................................
Ftl2-001_NCBIM37   408 ............................................................
Ftl2-001_CAST      408 ............................................................

                       *                                    *
Ftl1-001_NCBIM37   661 GGGGCCACAACCAGCGCAGACTGGCGCGCCCCAGGGGTCTCTGGGCGAGTATCTCTTTGA
Ftl1-001_CAST      661 A...................................A.......................
Ftl2-001_NCBIM37   468 A...................................A.......................
Ftl2-001_CAST      468 A...................................A.......................


Ftl1-001_NCBIM37   721 GCGCCTCACTCTCAAGCACGACTAGGAGGCCTCTGTACCTTCCAAGGGGCTCCCCCCTCT
Ftl1-001_CAST      721 ............................................................
Ftl2-001_NCBIM37   528 .........................-----------------------------------
Ftl2-001_CAST      528 .........................-----------------------------------


Ftl1-001_NCBIM37   781 GCTCTGCACCAGCCCGCCCTGGGACCTCCACCTGAATGAACCTCTCAAGCCACTAGGCAG
Ftl1-001_CAST      781 ............................................................
Ftl2-001_NCBIM37       ------------------------------------------------------------
Ftl2-001_CAST          ------------------------------------------------------------


Ftl1-001_NCBIM37   841 CTTTGTAACCGCCCTGGAGCCTCTGTCAAGTCTTGGACCAAGTAAAAATAAAGCTTTTTG
Ftl1-001_CAST      841 ............................................................
Ftl2-001_NCBIM37       ------------------------------------------------------------
Ftl2-001_CAST          ------------------------------------------------------------


Ftl1-001_NCBIM37   901 AGACAGC
Ftl1-001_CAST      901 .......
Ftl2-001_NCBIM37       -------
Ftl2-001_CAST          -------
```

Figure S4 (continued)

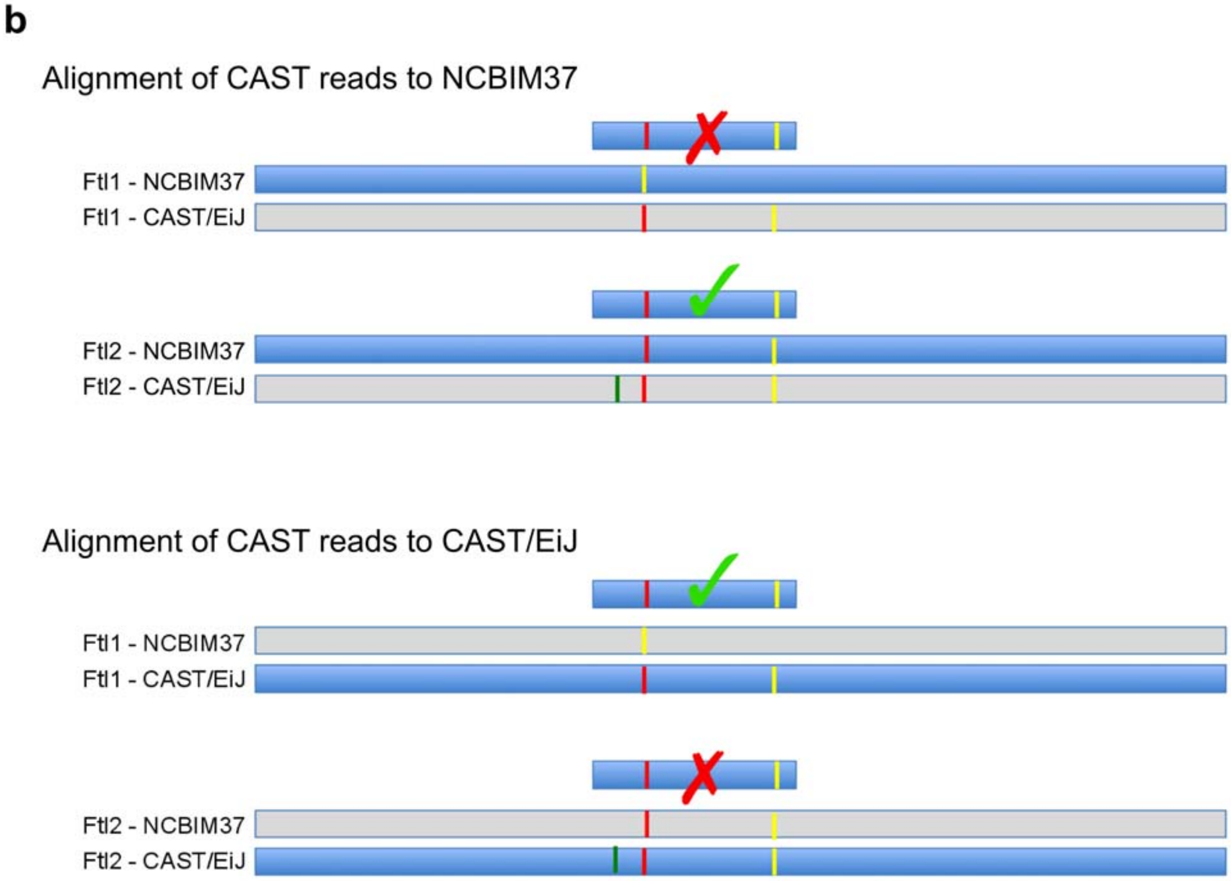

Figure S4 Strain polymorphisms between NCBIM37 and CAST in *Ftl1* and *Ftl2* transcript sequences can bias alignment of CAST-derived *Ftl1* reads. (A) Multiple alignment of *Ftl1-001* and *Ftl2-001* transcript sequences from NCBIM37 and the individualized CAST genomes. Variation in *Ftl1*/*Ftl2* abundance estimates in CAST liver RNA-seq stems mainly from 3-4 SNPs (starred). (B) Schematic showing how CAST polymorphisms in RNA-seq reads can cause misalignments in NCBIM37. CAST *Ftl1* reads that overlap any of these SNPs will align preferentially to *Ftl2* if aligned to NCBIM37 (upper panel). Accounting for CAST strain variation in *Ftl1* reduces spurious alignments to the *Ftl2* pseudogene (lower panel).

Figure S5

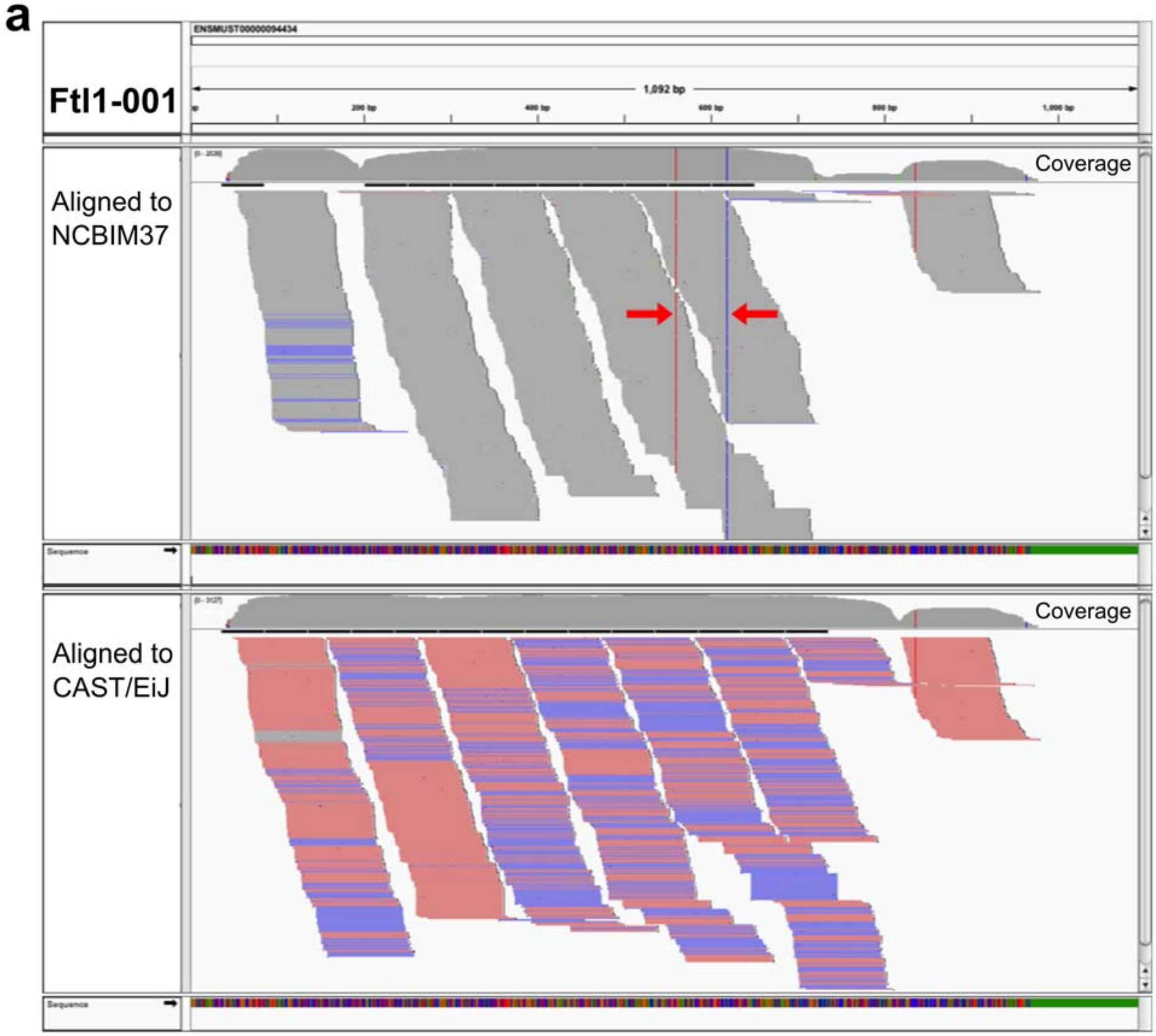
a
Ftl1-001
ENSMUST00000094434
1,092 bp
200 bp
400 bp
600 bp
800 bp
1,000 bp
Aligned to NCBIM37
Coverage
Sequence
Aligned to CAST/EiJ
Coverage
Sequence

Figure S5 (continued)

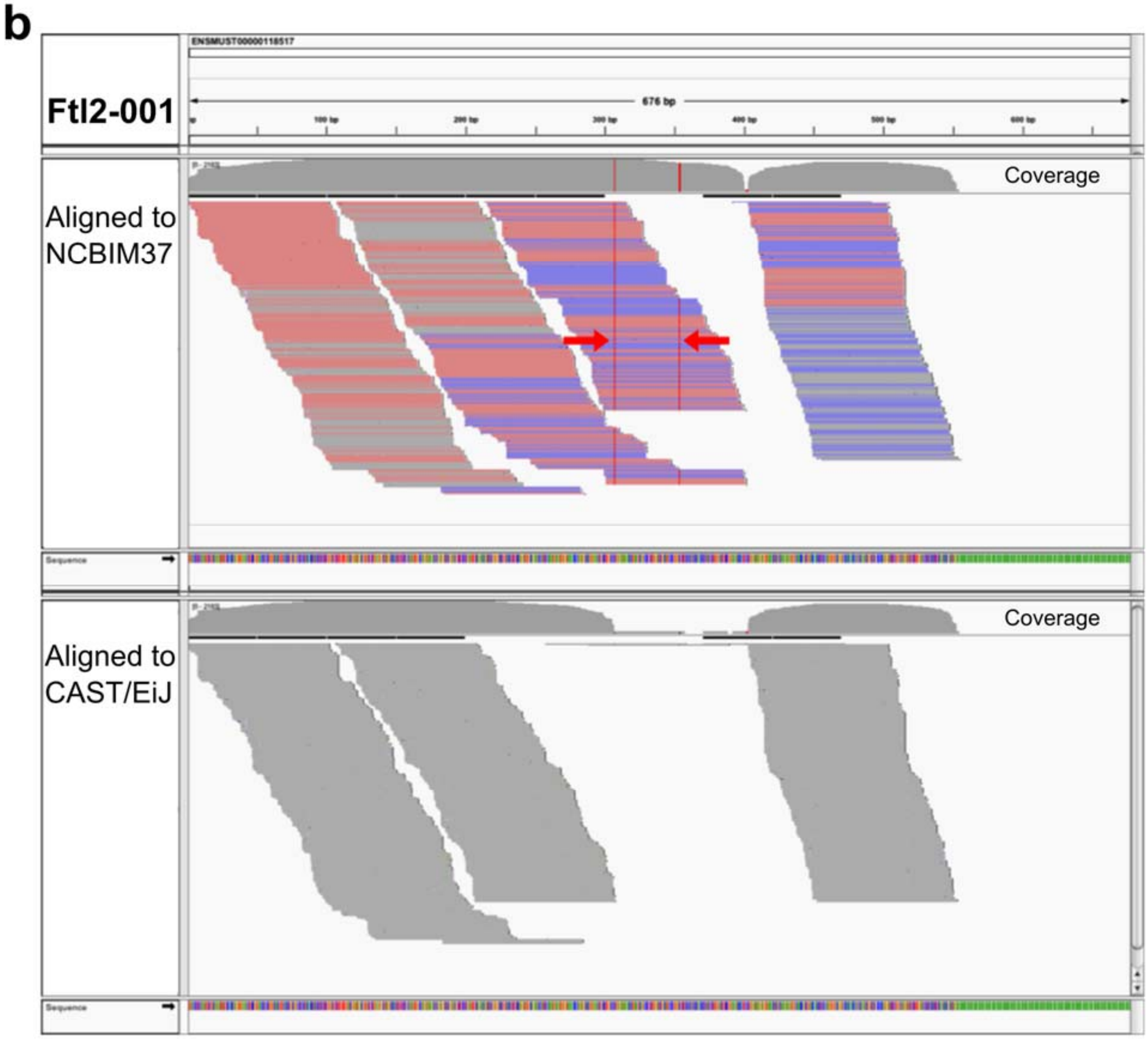

Figure S5 Coverage of CAST reads to *Ftl1* and *Ftl2* transcript sequences derived from the NCBIM37 reference genome and individualized CAST genome. Coverage plots show the distribution of CAST RNA-seq read alignments to *Ftl1-001* (A) and *Ftl2-001* (B) from alignment to each of the NCBIM37 reference and individualized CAST transcriptomes. Read coverage density (log transformed) is displayed at the top of each panel. For individual aligned reads, read color corresponds to orientation (red = forward strand, blue = reverse strand) and posterior probability. Gray reads have low probability of being transcribed from the aligned transcript location (as estimated by RSEM), while blue/red indicates reads that have been assigned high posterior probabilities. The red arrows point to SNPs in the CAST reads that differ from NCBIM37. Accounting for these CAST SNPs in the alignment diverts many reads from the *Ftl2* pseudogene to the parent protein-coding gene *Ftl1*.